

Research paper

Gypenoside XLIX alleviates sepsis-associated encephalopathy by targeting PPAR- α Panpan Zhao ^{a,1}, Wei Zhang ^{a,b,1}, Xinyu Zhou ^{c,1}, Yikun Zhao ^a, Aimin Li ^{a,*}, Yong Sun ^{a,*}^a Department of Neurosurgery, Institute of Neuroscience, The Affiliated Lianyungang Hospital of Xuzhou Medical University, Lianyungang Clinical College of Nanjing Medical University, The First People's Hospital of Lianyungang, Lianyungang 222000, China^b Jiangsu Key Laboratory of Marine Pharmaceutical Compound Screening, School of Pharmacy, Jiangsu Ocean University, Lianyungang 222005, China^c Department of Neurology, The First Affiliated Hospital of Kangda College of Nanjing Medical University, The Affiliated Lianyungang Hospital of Xuzhou Medical University, Lianyungang 222000, China

ARTICLE INFO

Keywords:

Sepsis
Brain
PPAR- α
Inflammation
Oxidative stress
Apoptosis

ABSTRACT

Sepsis-related systemic inflammation is a deadly condition with high rates of morbidity and mortality. There is evidence that sepsis affects the brain, and the most frequent organ dysfunction linked to sepsis is sepsis-associated encephalopathy. Sepsis-related brain damage can drastically reduce a patient's chances of survival. However, a specific treatment for sepsis-associated encephalopathy is not currently available. Consequently, to treat the brain damage caused by sepsis, investigating novel therapeutic strategies is imperative. After establishing the CLP-induced mouse SAE model, we treated the mice with Gyp-XLIX and evaluated apoptosis, neuroinflammation, brain damage, and oxidative stress in the brain tissue of each group of mice. Furthermore, the protective effects of Gyp-XLIX on LPS-treated BV-2 cells were assessed. We discovered that Gyp-XLIX treatment increased the survival rate of CLP-treated mice, alleviated SAE-related cerebral nerve abnormalities, and decreased blood–brain barrier breakdown, all of which could better preserve brain tissue in vivo. Furthermore, we identified associated proteins and found that Gyp-XLIX may reduce oxidative stress, cell apoptosis, and inflammation in the brain tissues of SAE mice. This observation was further validated in vitro. We established that Gyp-XLIX alleviates SAE by targeting PPAR- α . These findings may be important for the clinical applicability of Gyp-XLIX in SAE treatment. We found that Gyp-XLIX can alleviate brain injury in SAE by targeting PPAR- α and is a potential protective agent for SAE.

1. Introduction

Sepsis is a common condition and one of the main reasons critically ill individuals die, with up to 30 million infections worldwide each year (Kumar et al., 2019). Patients experience multiorgan failure as sepsis worsens, with the central nervous system being one of the most vulnerable organs (Pan et al., 2022); this system is most susceptible during the early stages of sepsis and progresses to sepsis-associated encephalopathy (SAE) (Meneses et al., 2019; Song and Zhou, 2022; Wu et al., 2021). According to previous studies, up to 70 % of patients with sepsis are clinically affected with SAE, and patient mortality increases with the severity of SAE (Song et al., 2023). Clinically, SAE is characterized by a rapid decline in cognitive function and has been reported to be accompanied by long-term neurocognitive impairment of memory,

learning, and behaviour. Despite its high prevalence and clinical relevance, only a few therapeutic options are available for treating SAE, such as basic supportive therapy and anti-infective therapy alone (Ding et al., 2022); therefore, exploring the mechanisms of brain damage in the context of sepsis would be helpful in developing strategies for the treatment of SAE.

One of the main effects that survivors of sepsis experience is impaired cognition. Previous reports have shown that the mechanisms of SAE are complex and multifactorial, with key mechanisms including blood–brain barrier (BBB) disruption and neuroinflammatory responses, including excessive microglial activation (Pu et al., 2022; Wen et al., 2022). One of the first and most significant steps in the development of SAE is systemic inflammation, and an increasing number of studies have reported that sepsis compromises the integrity of the BBB (Mei et al.,

* Corresponding authors.

E-mail addresses: liaimin6529@hotmail.com (A. Li), sunyong@njmu.edu.com (Y. Sun).¹ These authors contributed equally to this work.

2021). Increased BBB permeability is believed to be a primary factor in end-stage damage that results in death in severely ill sepsis patients (Zaky et al., 2021).

The macrophages of the central nervous system, known as microglia, are essential for both normal brain growth and neuronal regeneration. There is increasing evidence that microglia are critical to the pathophysiology of SAE (Michels et al., 2014). During sepsis, microglia are overactivated, and inflammatory cytokines are produced in large quantities, perpetuating the vicious cycle that leads to brain damage and results in the progression of SAE. In summary, the inhibition of neuroinflammation in the brain is important for alleviating septic encephalopathy.

Peroxisome proliferator-activated receptor α (PPAR- α) is a nuclear receptor that regulates the inflammatory response (Caillaud et al., 2021). PPAR- α is expressed in the brain and other organs and is crucial for inflammation, energy homeostasis, mitochondrial fatty acid metabolism, and oxidative stress (Wójtowicz et al., 2020). In rodent models of numerous neurological conditions, including experimental autoimmune encephalomyelitis, Parkinson's disease, and Huntington's disease (HD), the activation of PPAR- α causes anti-inflammatory effects that are advantageous (Esmaili et al., 2016). Recently, exogenous PPAR- α agonists were shown to reduce pain and protect neurons in both human and animal models of chronic neuropathic pain and inflammation (Oliveira et al., 2007). These studies suggest that PPAR- α activation may be effective in the treatment of neurological diseases.

Gynostemma pentaphyllum Makino, sometimes called five-leaf ginseng (Zhang et al., 2021c), is an edible herb or folk dietary supplement (Weng et al., 2021). It has garnered much interest lately because of its multiple pharmacological effects, such as triglyceride, antioxidant, anti-inflammatory, antiapoptotic, and antitumour effects, coupled with its low toxicity (Shin et al., 2014; Shin et al., 2015; Zhao et al., 2017). *Gynostemma* saponin is the main bioactive constituent of *Gynostemma* and is predicated on many cellular and animal models. *Gynostemma* saponin has a range of neuroprotective properties; for example, it can protect neonatal rat subventricular zone neural stem cells in the subventricular zone of the newborn rat brain prenatally exposed to ethanol (Dong et al., 2014), in addition to guarding against oxidative damage to substantia nigra neurons in a Parkinson's disease model (Wang et al., 2010), in contrast to neural stem cells in the stroke-affected ischaemic brain (Wang et al., 2014). In addition, giberellin saponins have been reported to reverse depressive or anxious behaviours by inhibiting neuroinflammation (Dong et al., 2018). These studies indicate that gypenosides have broad prospects in the prevention and treatment of brain diseases. Gypenoside XLIX (CAS number: 94987-08-3) is the main saponin in gypenoside, accounting for 6–20 % of the total saponins (Guo et al., 2017; Huang et al., 2007). This compound was discovered in *Gynostemma* in 1983 by a Japanese scholar, Tsuneematsu Takemoto, and was structurally characterized and confirmed to constitute the highest content of the active ingredient (Zhao et al., 2022). This component has not been reported in other families of plants and has also been a hot topic in the study of the chemical composition of *Gynostemma* saponins in recent years. Given its excellent neuroprotective qualities, we hypothesized that Gyp-XLIX could prevent SAE, but the specific mechanisms involved are still unclear and need to be further investigated.

2. Materials and methods

2.1. Chemicals and reagents

Gypenoside XLIX (Gyp-XLIX, purity >98 %, CAS: 94987-08-3, PUSH BIO-TECHNOLOGY) was used. LPS (*Escherichia coli* 0111: B4) was purchased from Sigma-Aldrich (MO, USA). Antibodies against GAPDH (60004-1-Ig, 1:50000), Nrf2 (16396-1-AP, 1:2000), Bax (50599-2-Ig, 1:2000), GFAP (16825-1-AP, 1:500), and NSE (66150-1-Ig, 1:800) were purchased from Proteintech (Wuhan, China). Antibodies against iNOS

(A3374, 1:1000), COX-2 (A3560, 1:1000), and Keap1 (A25297, 1:1000) were purchased from ABclonal (Wuhan, China). Antibodies against Bcl-2 (WL01556, 1:1000), PPAR- α (WL00978, 1:1000), and TLR4 (WL00196, 1:1000) were obtained from Wanleibio (Shenyang, China). Antibodies against IBA1 (GB114490-100, 1:500; GB12105-100, 1:1000) were obtained from Servicebio (Wuhan, China). Antibodies against p38 MAPK (8690), SAPK/JNK (9252), p-p38 (4511), and p-SAPK/JNK (4668) were purchased from Cell Signalling (MA, USA). Anti-mouse (SA00001-1) and anti-rabbit (SA00001-2) horseradish peroxidase-conjugated secondary antibodies were purchased from Proteintech. FITC-labeled goat anti-rabbit IgG(H + L) (E031220-01, 1:200), Cy3-labeled goat anti-mouse IgG(H + L) (E031610-01, 1:500), FITC-labeled goat anti-mouse IgG(H + L) (E031210-01, 1:200), and Cy3-labeled goat anti-rabbit IgG(H + L) (E031620-01, 1:500) were obtained from EarthoX (Beijing, China).

2.2. Experimental grouping and animal model establishment

Over a period of one week, C57BL/6 mice (aged 6–8 weeks, Pizhou Oriental Breeding Co., Ltd., Xuzhou) were selected and housed under standard conditions with a 12/12-h light/dark cycle (light hours of 7:00–19:00).

SAE was induced by caecal ligation and puncture (CLP) (Yin et al., 2023). As the industry standard for sepsis investigations, the CLP model is the most widely used experimental model of sepsis (Song et al., 2023). Experimentally, the mice were split into four groups at random: (1) the sham group; and the mice underwent CLP and after 4 h they received: (2) a daily saline injection for 5 days (CLP group); (3) a daily intraperitoneal injection of Gyp-XLIX 40 mg/kg for 5 days (CLP + Gyp-XLIX group); (4) a daily intraperitoneal injection of dexamethasone 2 mg/kg for 5 days (CLP + DEX group) (Cassol et al., 2010); (5) an intraperitoneal injection of Gyp-XLIX 40 mg/kg, then 0.5 h later injected daily with 2 mg/kg PPAR- α inhibitor-GW6471 for 5 days (CLP + Gyp-XLIX+GW6471 group).

The process of CLP can be summarized as follows: Mice were fixed on a flat plate after being anaesthetized. After shaving, cleaning, and disinfecting the abdominal skin, a longitudinal incision was made along the midline of the abdomen. The top end of the caecum was then gently pushed to fill it in after it was exposed through the abdominal incision. Using a sterile 18-G needle, the distal caecum was pierced, and 50 % of the caecum was ligated with No. 3 silk. To guarantee a smooth perforation, a tiny amount of faeces was extruded. Following its replacement within the abdominal cavity, the caecum was sealed and sterilized. The ceca of the mice in the sham-operated group had their caecums gently removed and placed back into their abdominal cavities, without any kind of treatment. After that, the abdomen was sutured and sterilized, and the mice were placed in a thermostatic blanket until they woke up. At the end of the operation, all of the mice were subcutaneously injected with 1 mL of recovery saline solution, and antibiotics were not used. The mice were given the reagent injections for 5 days and monitored every day for survival, behaviour, and condition. At the end of the experiment, all of the mice were euthanized, the whole brain was collected, and the cerebral cortex was separated for additional experiments. The experimental procedures are shown in Fig. 1A.

Furthermore, we took great care to reduce both the quantity and suffering of the animals employed. All animal experiments were approved by the Institutional Animal Ethics Committee of Jiangsu Ocean University, and animal care was performed in accordance with institutional guidelines.

2.3. Neurological deficit test

An investigator blinded to the group assignment conducted the neurological evaluations. The Longa test is used for this assessment: Grade 0, with no neurological deficits (normal) in symptoms; Level 1, the left front paw cannot be extended when the mouse's tail is lifted

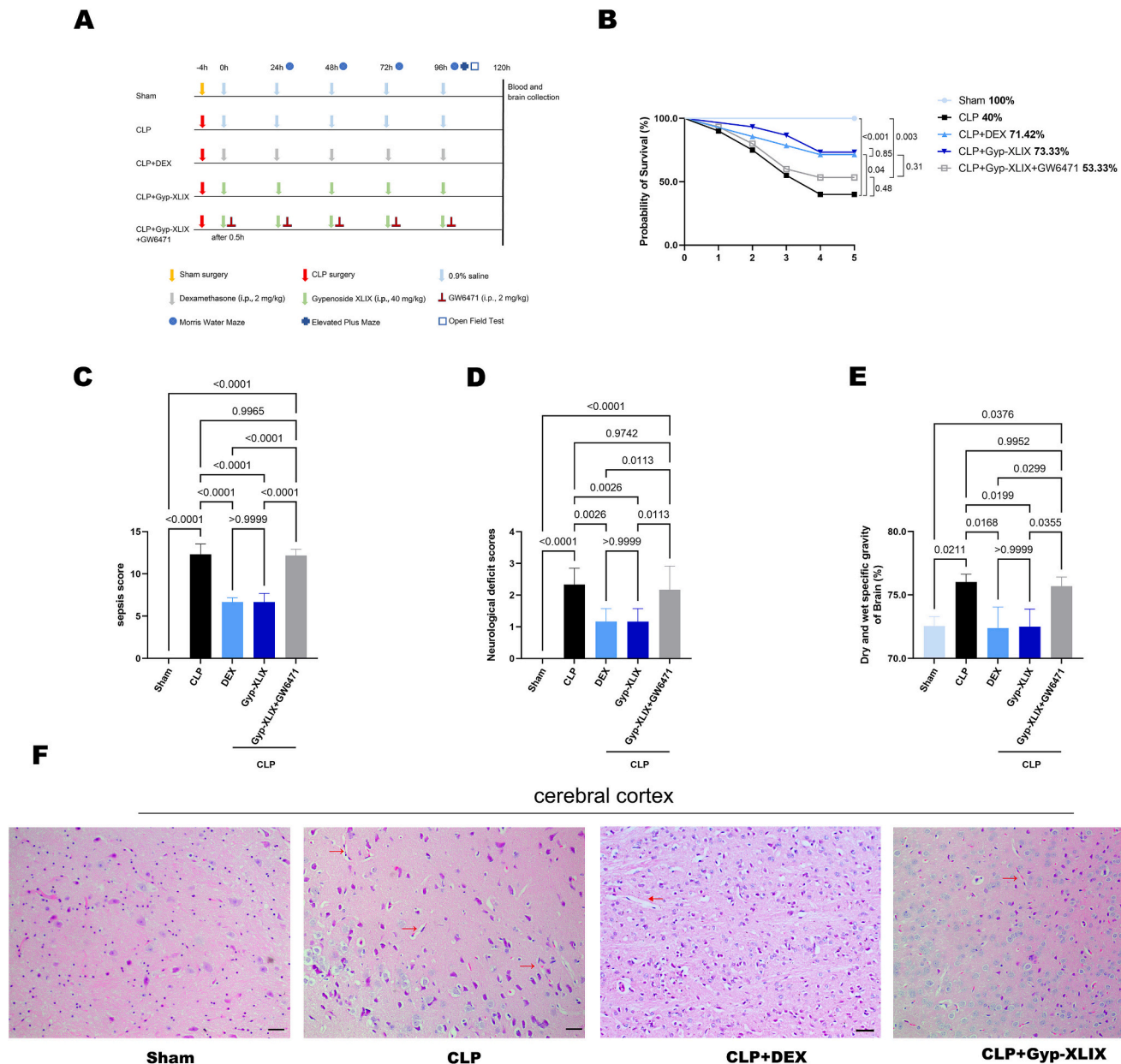


Fig. 1. Gypenoside XLIX can improve brain injury in septic mice. (A) The whole experimental process schedule. (B) The number of mice that survived in each group was noted, $n = 15$. (C) Mice in each group were subjected to the sepsis model score, $n = 6$. (D) Neurological deficit scores were performed on mice in each group, $n = 6$. (E) Edema of mouse brain tissue was detected, $n = 3$. (F) Histopathological changes in the cerebral cortex were observed using HE staining, $n = 3$. Scale bar = 100 μm .

(mild); Grade 2, hovering to the left when walking (moderate); Grade 3, difficulty walking, tilting to the left (severe); and Grade 4, cannot walk spontaneously (very severe) (Guo et al., 2019).

2.4. Brain water content

Wet and dry gravity methods were used to determine the water content of the brain (Tang et al., 2017). The mice were euthanized, the whole brains were extracted, and their wet weights were recorded. The brain samples were then dried in an oven at 80 °C for 48 h to determine their dry weight. Using the previously described method, the brain samples were weighed via an analytical scale to calculate their wet weight. The brain water content was calculated using the following formula: $(\text{wet weight} - \text{dry weight}) / \text{wet weight} \times 100\%$ (Lee et al., 2024).

2.5. BBB permeability assessment

BBB integrity was assessed by measuring the Evans blue (EB) content. One hour before the brains were removed, EB dye (2 % saline solution, 4 mL/kg) was injected into the tail vein. The two cerebral hemispheres were then rapidly divided on ice, weighed individually, and homogenized in 1.5 mL of 50 % trichloroacetic acid solution. Absolute ethanol was used to dilute the supernatant four times following centrifugation (13,600 $\times g$, 20 min). The absorbance value was determined via a fluorescence spectrophotometer (excitation wavelength: 620 nm; emission wavelength: 680 nm). Micrograms of EB per gram of brain tissue constitute the unit of measurement for EB content in brain tissue extracts. Similarly, EB dye leakage was also observed via a fluorescence microscope using blue excitation light (Guo et al., 2019).

2.6. Elevated plus maze

The elevated plus maze (EPM) was used to assess cognitive impairment (Gao et al., 2022). The EPM is based on an animal's spontaneous fear-like reflex, which is an unconditioned reflex model and an internationally recognized method for measuring anxiety responses (Li et al., 2023). The EPM has a square central space (6×6 cm), with a wall thickness of 15 cm, two open arms (35×6 cm) and two closed arms (35×6 cm). After the mouse was placed facing the closed arm on a central platform, it was allowed to roam about at will for five minutes. The maze was washed with 75 % ethanol after every trial. The automated tracking software of the animal motion monitoring system was utilised to capture and examine the activities of every mouse. The number of times the mouse entered the maze arms and the time spent in each maze arm were recorded. As mentioned earlier, we used the MWM and EPM tests to detect behavioural changes.

2.7. Morris water maze

The Morris water maze (MWM) is commonly used to assess cognitive impairment (Gao et al., 2022). Based on previous studies, we assessed the cognitive function of spatial learning and memory in the mice in each group via the MWM test (Li et al., 2022). In brief, the mice were placed in a circular pool of water at a temperature of 24 ± 1 °C. A transparent platform is placed in the water, 2 cm below the surface. The mouse was positioned with its back to the wall and allowed 60 s to find the submerged platform. Computer software was used to monitor and record every mouse action. The mice did not die from their wound infection during the water maze test.

2.8. Open field test

The open field test was conducted according to previously described methods (Reis et al., 2022). The mice were placed in a laboratory chamber ($100 \times 100 \times 70$ cm container) for 5 min. The distance travelled and the number of times they crossed the intermediate area were tracked and measured to assess their motor ability. The apparatus was cleaned with 75 % alcohol between tests to remove odour cues.

2.9. Cell culture

The Chinese Academy of Medical Sciences (Beijing, China) provided the mouse microglial cell line BV-2. The cells were cultured at 37 °C/5 % CO₂ in 10 % DMEM (Servicebio, Wuhan, China) supplemented with 10 % FBS (Biological Industries, Israel) and 1 % penicillin and streptomycin solution. Before usage, LPS was stored at -80 °C after being dissolved in DMEM at a concentration of 1 µg/mL as a stock solution. Four different experimental groups were subsequently established for follow-up experiments: the control group, the LPS group, the LPS + Gyp-XLIX treatment group, and the LPS + Gyp-XLIX+GW6471 (a specific inhibitor of PPAR- α , Abmole) treatment group. BV-2 cells were pretreated with 10 µM Gyp-XLIX before LPS stimulation, and after 12 h, they were stimulated with 1 µg/mL LPS. After 24 h, the cells were harvested for testing. In accordance with previous studies, the LPS + Gyp-XLIX+GW6471 treatment group was pretreated with the PPAR- α antagonist GW6471 (5 µM) for 30 min, treated with Gyp-XLIX for 12 h, and finally stimulated with LPS (Zhou et al., 2022).

2.10. CCK8

The CCK8 test (Biosharp, Beijing, China) was used to measure the viability of the BV-2 cells in accordance with the manufacturer's instructions. BV-2 cells were seeded at a density of 1×10^5 cells/mL in 96-well plates and treated with various concentrations of Gyp-XLIX (0, 10, 20, 30, or 40 µM). Each well received 10 µL of CCK8 reagent. After an hour, the absorbance value at 450 nm was determined to determine the

viability of each group of cells.

2.11. NO detection

The Griess reagent test (Promega, USA) was used to measure NO production. In brief, 50 µL of N-1-naphthylethylenediamine dihydrochloride (NED) solution was added after 50 µL of cell culture supernatant had been combined for 10 min with an equal volume of sulfanilamide solution. Finally, a plate reader was used to measure the absorbance at 540 nm to determine the amount of NO.

2.12. ROS detection

To identify intracellular ROS generation, the Reactive Oxygen Species Assay Kit (Biosharp, Beijing, China) was used, and the manufacturer's instructions were carefully followed. 2',7'-Dichlorofluorescein diacetate (DCFH-DA) is degraded enzymatically by intracellular esterases to form nonfluorescent DCFH, which easily crosses the cell membrane. ROS then oxidise the DCFH to generate highly fluorescent 2',7'-dichlorofluorescein (DCF). The amount of ROS produced is closely correlated with the fluorescence intensity.

2.13. Biochemical assay

The animals were euthanized, and the brains were immediately excised, followed by cerebral cortex isolation. The cerebral cortex was weighed and homogenized with 9 times the volume of isotonic saline. Following centrifugation, the supernatant was obtained and utilised to detect relevant indicators. Oxidative stress indicators, including total antioxidant capacity (T-AOC, A015-1-1, the ferric reducing ability of the plasma method), catalase activity (CAT, A007-1-1, the ammonium molybdate method), glutathione peroxidase activity (GSH-Px, A005-1-2, the colorimetric method), and malondialdehyde content (MDA, A003-1-2, the TBA method), were detected via kits from Nanjing Jiancheng Technology Co., Ltd.

2.14. Histological evaluation (HE)

Fresh cerebral cortex tissue was obtained, washed in PBS, and sliced into thin sections. The sections were then fixed in a 4 % paraformaldehyde solution (Biosharp, Beijing, China) for 12 h to preserve the original brain structure. The sections were subsequently dehydrated via a graded ethanol series and embedded in paraffin. Prior to staining, the sections were dewaxed with xylene and stained with haematoxylin for several minutes. Pathological changes in each group were further examined by observing the morphological changes in the brain tissue via optical microscopy.

2.15. Immunofluorescence

The frozen slices of cerebral cortex were baked in an oven at 37 °C for 10 min to control moisture. Then it was fixed in 4 % paraformaldehyde solution for 30 min, and washed in PBS buffer for 3 times for 5 min each time. Antigen repair was performed using EDTA antigen repair solution (pH 9.0). After natural cooling, the frozen slices were washed 3 times in PBS for 5 min each time. After the sections were slightly dried, draw circles around the tissues with an immunohistochemical pen, add 3 % BSA to seal them, and seal them for 30 min. Then the slices were incubated with primary antibodies at 4 °C overnight in a wet box, second antibodies at room temperature for 60 min, 2 µg/mL DAPI at room temperature for 10 min, and autofluorescence quencher B solution for 5 min. Finally, the slices were sealed with anti-fluorescence quencher sealant. Images are observed and acquired under confocal microscopy.

2.16. Real-time PCR detection

TRIzol (CW0580S; CWBIOTECH, Beijing, China) was used for total RNA extraction and subsequent cDNA synthesis via reverse transcription. rtPCR was performed to detect the cDNA, which was combined with MonAmp SYBR Green qPCR Mix (MQ10101, Monad, Suzhou, China), RNase-free water, and upstream and downstream primers. The primers were designed on the basis of information from previous studies and were provided by Sangon Biotech (Shanghai, China) (Zhang et al., 2023b). The primers for the inflammatory cytokines were as follows: MM-Actb-F: GCCATGTACGTAGCCATCCA; MM-Actb-R: ACGCACGATTTCCCTCTCAG; MM-IL-1 β -F: TGCCTTCTTGGGACTGATGC; MM-IL-1 β -R: GCAAGTGCATCATCGTTGTTTC; MM-iNOS-F: GGTGAAGG-GACTGAGCTGTTA; MM-iNOS-R: TGAAGAGAACTTCCAGGGGC; MM-IL-10-F: TAACTGCACCCACTTCCCAG; MM-IL-10-R: AAGGCTTGG-CAACCCAAGTA; MM-TNF- α -F: GACGTGGAAGTGGCAGAAGA; MM-TNF- α -R: GGCTACAGGCTTGTCACCTCG. The expression of Actb was used for normalization. The relative mRNA expression of the target gene was assessed via the $2^{-\Delta\Delta C_t}$ method (Zhang et al., 2021b).

2.17. Western blot analysis

Protein was extracted with RIPA lysis buffer supplemented with 1 % PMSF and 1 % phosphatase inhibitor. The protein concentration was determined via the BCA method and adjusted with RIPA buffer. To prepare for western blot analysis, the material was combined with loading buffer and heated for ten minutes at 100 °C in a water bath. After being separated by 10 % SDS-PAGE, the protein sample was transferred onto a PVDF membrane. After the membrane was blocked for an hour at room temperature with TBST containing 5 % skim milk powder, it was incubated with the corresponding primary antibody at 4 °C overnight. After that, the membrane was incubated for 1.5 h at room temperature with the secondary antibody. A multifunctional, ultrasensitive imaging system (SHST, Shanghai, China) was used to photograph the protein bands, which were visualized via an improved chemiluminescent reagent (Vazyme, Nanjing, China). Using GAPDH as an internal reference, quantitative analysis was carried out using ImageJ software to determine the relative expression levels of each protein (Zhang et al., 2023a).

2.18. Tunnel staining

Paraffin embedded tissue sections of cerebral cortex were successively dewaxed in xylene, soaked in anhydrous ethanol, soaked in gradient ethanol (90 %, 80 %, 70 %), soaked and rinsed. Then, the brain tissue was circled with an immunohistochemical pen and permeated in Proteinase K solution of 20 μ g/mL at room temperature for 20 min. According to the manual of TUNEL BrightRed Apoptosis Detection Kit (Vazyme, Nanjing), brain tissue apoptosis staining was performed. Specifically, equilibration was performed with 1 \times Equilibration Buffer at room temperature for 10 min, incubation with 50 μ L of incubation buffer containing TdT enzyme at 37 °C for 60 min and staining with 2 μ g/mL DAPI at room temperature for 5 min. Finally, the anti-fluorescence quencher cover is added. BrightRed fluorescence was observed at 620 \pm 20 nm. Blue fluorescence of DAPI was observed at 460 nm. In the apoptotic nucleus there is red fluorescence produced by the incorporation of BrightRed.

2.19. Bioinformatics analysis

We used bioinformatics to investigate the role of PPAR- α in the process of brain injury in sepsis. The GEO database is an open functional genomic database for obtaining transcriptional profiling datasets (GSE131761). The GSE131761 microarray data are based on the GPL13497 platform. We downloaded the transcription and expression profiles of healthy people and sepsis patients in MINiML format, which contained the complete data of all platforms, samples and GSE records in

the GSE; log2 values were uniformly processed for the datasets that were not normalized, and the final results were visualized (Barrett et al., 2013; Zhang et al., 2019).

2.20. Statistical analysis

GraphPad Prism 8.0 software was used to conduct the statistical analysis. The Shapiro–Wilk test was used to determine the distribution of the data, and all of the data that conformed to a normal distribution were analyzed via one-way ANOVA, followed by the use of the Tukey post hoc test to compare variables between groups. Error bars represent the mean \pm standard deviation (SD). *: CLP group vs. Sham group/Control group vs. LPS group, * P < 0.05, ** P < 0.01, *** P < 0.001; #: CLP group vs. DEX-treated CLP group, Gyp-XLIX-treated CLP group/LPS group vs. LPS + Gyp-XLIX treatment group, # P < 0.05, ## P < 0.01, ### P < 0.001. \$: LPS + Gyp-XLIX treatment group vs. LPS + Gyp-XLIX+GW6471, \$ P < 0.05, \$\$ P < 0.01, \$\$\$ P < 0.001.

3. Results

3.1. Gyp-XLIX can ameliorate brain damage in mice with sepsis

To investigate whether Gyp-XLIX could be used to treat brain damage caused by sepsis, a mouse model of CLP sepsis was used (Fig. 1A). The effective dosage of gypenoside XLIX was determined as shown in Fig. S1. After model establishment, the condition of the mice in the Sham group was not different from that of the normal mice. Compared with the Sham group, the CLP group presented obvious characteristics of sepsis, including shortness of breath, body curl, a decrease in skin temperature and other symptoms. The mice in the dexamethasone administration group and the Gyp-XLIX administration group were clinically improved relative to the CLP group. The main manifestations were increased activity, increased amounts of food and water consumed, decreased respiration, increased skin temperature, and no secretions on the body surface. In addition, after the inhibition of PPAR- α with GW6471 in CLP + Gyp-XLIX mice, the status of this group of mice became worse than that of CLP + Gyp-XLIX mice, indicating obvious symptoms of sepsis.

Analysis of the survival of the mice in each group revealed that, compared with the Sham group, the CLP group's survival rate decreased (F = 1.591, P < 0.001). The survival rate of the CLP mice improved after the injection of Gyp-XLIX (F = 1.591, P = 0.04), whereas the survival rate did not differ from that of CLP + DEX mice (F = 1.591, P = 0.85), suggesting that the therapeutic effect of Gyp-XLIX was similar to that of DEX. Compared with those in the CLP + Gyp-XLIX group, the survival rates of the CLP + Gyp-XLIX+GW6471 group were lower after the administration of GW6471 (F = 1.591, P = 0.31) (Fig. 1B). In conclusion, the sepsis model scores of each group demonstrated the same outcomes (Fig. 1C).

CLP mice displayed clear neurological damage during sepsis. Specifically, the neurological impairment score of the CLP group was much greater than that of the Sham group (F = 22.64, P < 0.0001), whereas the neurological impairment score of the CLP group was dramatically lower in response to dexamethasone and Gyp-XLIX treatment (F = 22.64, P = 0.0026; F = 22.64, P = 0.0026). Notably, CLP + Gyp-XLIX+GW6471 mice showed an increase in neurological dysfunction scores compared with CLP + Gyp-XLIX mice (F = 22.64, P = 0.0113) (Fig. 1D). These findings suggest that Gyp-XLIX and dexamethasone may have protective effects on brain function. Similarly, the brain water content of the CLP group was noticeably greater than that of the Sham group (F = 8.359, P = 0.0211). Compared with that in CLP mice, cerebral oedema was reduced during Gyp-XLIX therapy (F = 8.359, P = 0.0199). There was no significant difference between the CLP + Gyp-XLIX treatment group and the CLP + DEX group in cerebral oedema (F = 8.359, P > 0.99), indicating that Gyp-XLIX has the same therapeutic effect as DEX in this process. In contrast, the injection of GW6471 in CLP

+ Gyp-XLIX mice significantly increased brain oedema ($F = 8.359$, $P = 0.0355$). (Fig. 1E).

Subsequently, sections of the cerebral cortex stained with HE were examined to ascertain whether pathological changes were present in each group. As shown in Fig. 1F, compared with the Sham group, the CLP group presented obvious structural damage to the cerebral cortex, accompanied by microglial hyperplasia, and many elongated and irregular nuclei were observed. Interestingly, compared with that in the CLP group, the damage to the cortex in the DEX-treated group was alleviated, and the proliferation of microglia was reduced. In addition, after treatment with Gyp-XLIX, the morphological and structural damage to the cerebral cortex caused by SAE returned to normal, and the proliferation of microglia decreased, indicating that Gyp-XLIX can restore the structure of the cortex and have the same effect as DEX. These results all indicate that Gyp-XLIX can improve the pathology of sepsis and inhibit the brain injury induced by sepsis to a certain extent.

3.2. Gyp-XLIX improves cognitive impairment and BBB destruction in CLP mice

To investigate the effects of CLP on cognitive function in mice, we conducted behavioural tests to evaluate cognitive function. First, we evaluated the behaviour of each group of mice in open field studies to eliminate the possibility that the corresponding alterations were from decreased motor activity in CLP mice. As shown in Fig. 2A-E, there was no difference in the movement speed or distance of the mice in each group ($F = 0.05681$, $P > 0.5$; $F = 0.2611$, $P > 0.5$), indicating that the experiment did not affect autonomous motor ability, which is consistent with the results of previous studies (Zhang et al., 2024). Interestingly, compared with those in the Sham group, the CLP group spent less time in the central region and travelled a shorter distance in the central region, suggesting brain damage after CLP ($F = 10.61$, $P = 0.0037$; $F = 7.261$, $P = 0.0150$). This phenomenon was significantly improved in the mice treated with Gyp-XLIX ($F = 10.61$, $P = 0.0176$; $F = 7.261$, $P = 0.0216$). Moreover, we did not observe a significant difference between the CLP + Gyp-XLIX and CLP + DEX groups ($F = 10.61$, $P = 0.9796$; $F = 7.261$, $P = 0.9820$), indicating that the therapeutic effect of Gyp-XLIX is similar to that of the positive control drug DEX.

The EPM test can be used to assess cognitive impairment (Gao et al., 2022). The results of the behavioural test (EPM) demonstrated that the CLP mice had decreased cognitive function; however, the cognitive performance of the CLP mice was enhanced by dexamethasone and Gyp-XLIX. Compared with the mice in the Sham group, the CLP group explored the open arms less and the closed arms more. Interestingly, compared with that of CLP mice, exploration in the open arms was greater after treatment with Gyp-XLIX and DEX. In the MWM experiment, CLP mice took longer to reach the platform than Sham mice did, but these phenomena were alleviated after Gyp-XLIX treatment. In addition, there was no significant difference in the improvement effect between Gyp-XLIX and DEX. These results indicated that CLP induced cognitive impairment in mice; however, dexamethasone and Gyp-XLIX treatment alleviated this cognitive impairment (Fig. 2F-I).

Next, we explored the possible mechanisms of CLP-induced cognitive impairment and revealed that BBB disruption is associated with the pathogenesis of SAE (Chen et al., 2020). Previous research has demonstrated that, in CLP models, BBB penetration increases. An azo dye called Evans blue (EB) can bind to albumin in the blood and is unable to pass across the BBB normally. Therefore, the degree of EB fluorescence in the brain is indicative of structural damage to the BBB. Therefore, to assess the degree of BBB damage, we injected EB into the tail vein. The findings of the amount of EB in each group of brain tissue and the immunofluorescence map demonstrated that the BBB integrity of the mice in the CLP group was inferior to that of the mice in the Sham group. Compared with the CLP group, the DEX group and the Gyp-XLIX group presented a reduction in CLP damage to the BBB (Fig. 2J-K).

MMP9 is one of the most important MMPs in the gelatinase family,

and the overexpression of MMP9 destroys the BBB. Claudins play an important role in maintaining the BBB in the brain. Therefore, we detected the protein expression of MMP9 and claudin to explore the BBB situation in each group. Compared with the Sham group, the CLP group presented significantly increased protein expression of MMP9 ($F = 9.791$, $P = 0.0084$) and decreased protein expression of claudin ($F = 11.01$, $P = 0.0022$). Compared with CLP, the addition of Gyp-XLIX significantly reversed the changes in the expression levels of these proteins, resulting in a decrease in the expression of MMP9 ($F = 9.791$, $P = 0.0057$) and an increase in the expression of claudin ($F = 11.01$, $P = 0.0213$). DEX also reversed the expression change in the CLP group but it did not significantly differ from that in the CLP + Gyp-XLIX group ($F = 9.791$, $P = 0.4865$; $F = 11.01$, $P = 0.9352$) (Fig. 2L-O). These results suggest that Gyp-XLIX may be used to treat CLP-induced brain injury in mice.

3.3. Gyp-XLIX inhibits the production of inflammatory mediators

One of the most important aspects of sepsis pathophysiology is neuroinflammation. The primary pathogenic sign after an increase in BBB permeability is the overproduction of inflammatory factors (Liu et al., 2023; You and Jiang, 2021). Numerous investigations have verified that CLP triggers a systemic inflammatory response and results in the release of a range of cytokines and immune factors (Yamashita et al., 2018). In the brain tissues of each group, we detected the mRNA expression levels of a few pro- and anti-inflammatory factors. Compared with sham mice, CLP animals presented higher expression levels of the proinflammatory factors *IL-1 β* ($F = 54.68$, $P < 0.0001$), *TNF- α* ($F = 11.06$, $P = 0.0002$), *IL-6* ($F = 61.19$, $P < 0.0001$), and *INOS* ($F = 49.82$, $P < 0.0001$) and a decreasing trend in the anti-inflammatory cytokine *IL-10* ($F = 14.58$, $P = 0.0006$). Following treatment with Gyp-XLIX, the expression levels of these inflammatory factors decreased ($F = 54.68$, $P < 0.0001$; $F = 11.06$, $P = 0.0030$; $F = 61.19$, $P < 0.0001$; $F = 49.82$, $P < 0.0001$), whereas the expression of *IL-10* increased ($F = 14.58$, $P = 0.0010$). Gyp-XLIX had the same anti-inflammatory effect as DEX ($F = 54.68$, $P = 0.9999$; $F = 11.06$, $P = 0.9992$; $F = 61.19$, $P = 0.9905$; $F = 49.82$, $P > 0.9999$; $F = 14.58$, $P = 0.3683$) (Fig. 3A-E). In addition, we detected the expression of the inflammation-related proteins iNOS, COX-2, TLR4 and p-p65 via western blotting. These proteins were markedly elevated following brain tissue damage in septic mice compared with Sham mice ($F = 25.18$, $P = 0.0010$; $F = 16.07$, $P = 0.0043$; $F = 8.011$, $P = 0.0118$; $F = 43.28$, $P < 0.0001$). The expression of these proteins was restored after the administration of Gyp-XLIX ($F = 25.18$, $P = 0.0003$; $F = 16.07$, $P = 0.0036$; $F = 8.011$, $P = 0.0155$; $F = 43.28$, $P < 0.0001$). In addition, there was no significant difference between Gyp-XLIX and CLP + DEX mice in alleviating the expression of inflammation-related proteins, indicating the same anti-inflammatory effect ($F = 25.18$, $P = 0.9723$; $F = 16.07$, $P = 0.6596$; $F = 8.011$, $P = 0.9599$; $F = 43.28$, $P = 0.1896$) (Fig. 3F-J). These results suggest that Gyp-XLIX exerts a significant anti-inflammatory effect during sepsis-induced brain injury.

3.4. Gyp-XLIX reduces oxidative stress during SAE

Furthermore, a biochemical kit was used to assess the effects of Gyp-XLIX on oxidative stress in SAE mice. As shown in Fig. 4A-D, compared with those in the Sham group, the MDA levels in the CLP group increased quickly ($F = 12.77$, $P < 0.0001$). Gyp-XLIX treatment reversed this phenomenon ($F = 12.77$, $P = 0.0059$), suggesting that Gyp-XLIX decreased the degree of membrane lipid peroxidation. In addition, the activities of three important antioxidant enzymes, SOD, T-AOC, and CAT, and the content of GSH were evaluated. The findings demonstrated that in mice with sepsis-induced brain injury, unlike those in Sham mice, the activity of these enzymes was decreased ($F = 10.75$, $P = 0.0067$; $F = 12.66$, $P < 0.0001$; $F = 11.21$, $P = 0.0005$); however, following medication therapy, the condition of the mice improved, and the activity of several antioxidant enzymes was restored ($F = 10.75$, $P = 0.0002$; $F =$

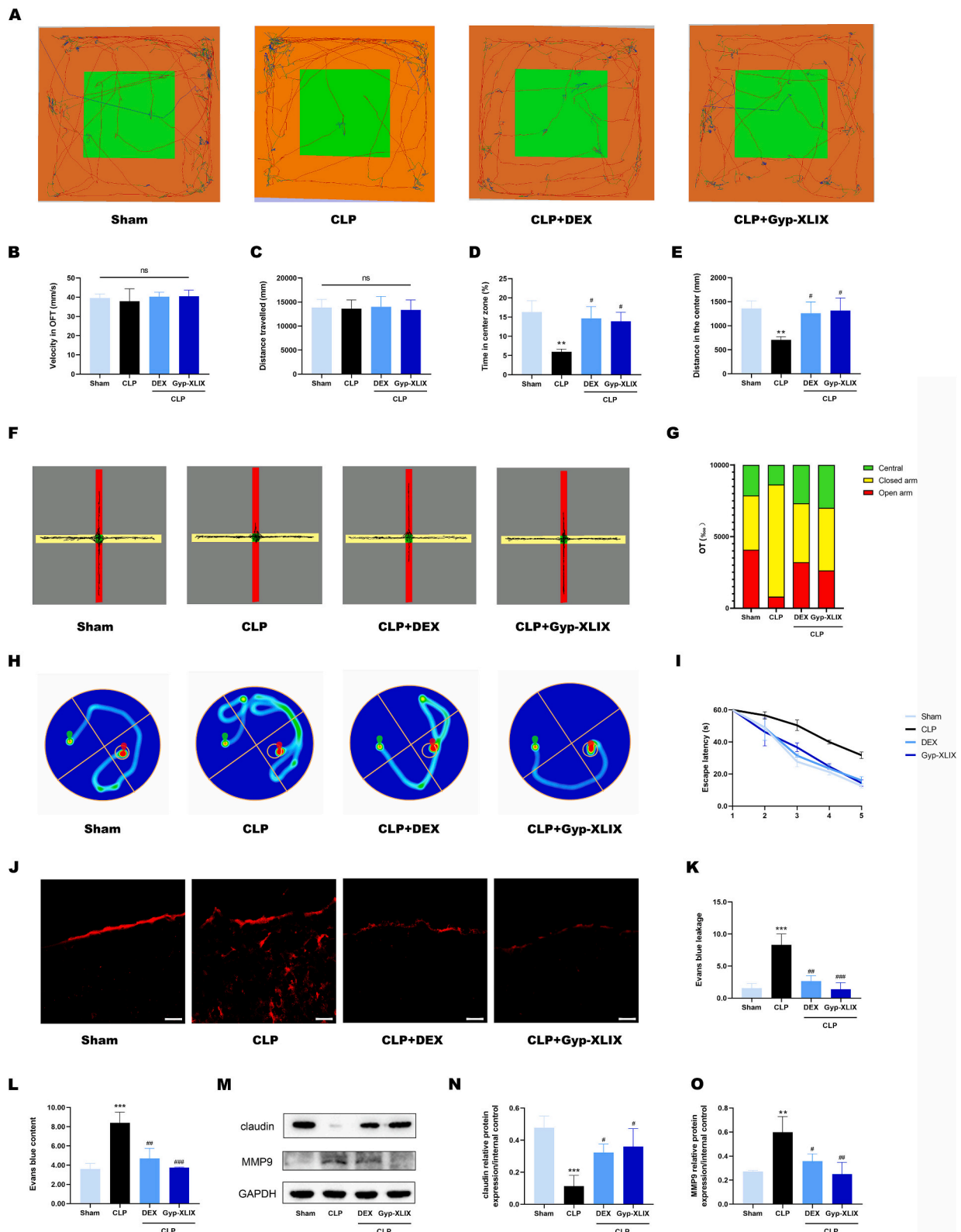


Fig. 2. Gypenoside XLIX improved cognitive impairment and BBB destruction in CLP mice. (A) Movement of the mice in an open field test, $n = 6$. (B) Movement speed of the mice in an open field test, $n = 6$. (C) The distance each group of mice moved in an open field test, $n = 6$. (D) The proportion of time spent in the central area by each group of mice, $n = 6$. (E) The distance each group of mice moved in the central region, $n = 6$. (F) The cognitive function of the mice in each group was analyzed via an EPM test, $n = 6$. (G) The time the mice entered the open arms in an EPM test, $n = 6$. (H) The swimming path of each group of mice in a MWM test, $n = 6$. (I) Escape latency of each group of mice in a MWM test, $n = 6$. (J) Confocal microscopy was used to observe EB leakage in the cerebral cortex, $n = 3$. The red fluorescence signal is EB, scale bar = 100 μm , and was quantified (K). (L) Evans blue content was detected in brain tissue, and the content of Evans blue extracted with formamide was quantified at 620 nm, $n = 3$. (M-O) The protein expression levels of claudin and MMP9 in the brain tissues of the mice in each group were detected via western blotting and normalized, and GAPDH was used as an internal control, $n = 3$. (For interpretation of the references to colour in this figure legend, the reader is referred to the web version of this article.)

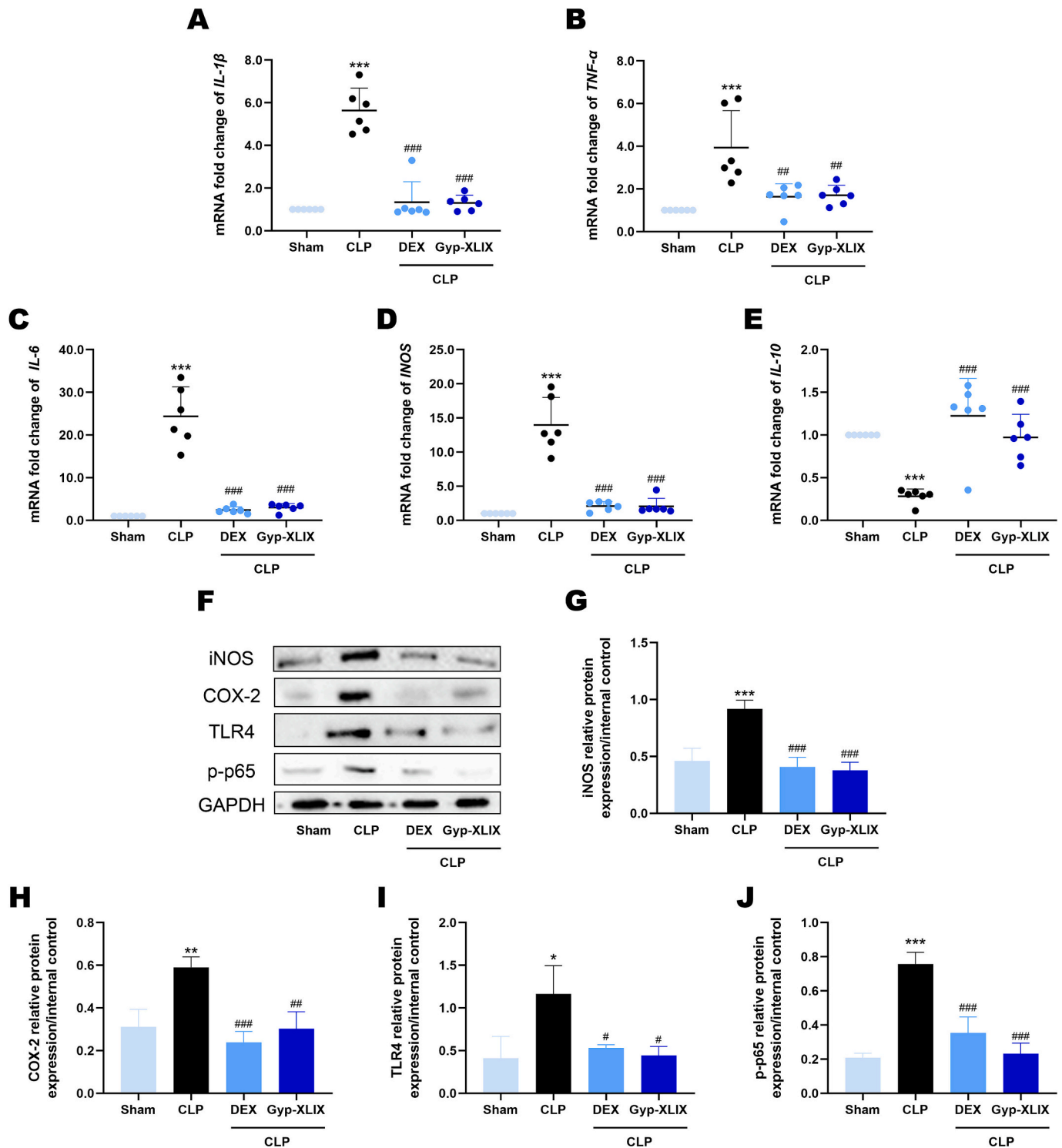


Fig. 3. Gypenoside XLIX inhibits the production of SAE-related inflammatory mediators. (A–E) RNA collected from brain tissue was reverse transcribed into cDNA, and the mRNA expression levels of *IL-1β*, *TNF-α*, *IL-6*, *iNOS*, and *IL-10* in each group were detected by QPCR, $n = 6$. (F–J) Expression levels of inflammation-associated proteins *iNOS*, *COX-2*, *TLR4*, and *p-p65* were determined using proteins isolated from brain tissue, $n = 3$.

12.66, $P = 0.0246$; $F = 11.21$, $P = 0.0004$). Similarly, the ability of Gyp-XLIX to regulate oxidative stress was not different from that of the positive control drug DEX ($F = 12.77$, $P = 0.7528$; $F = 10.75$, $P = 0.3417$; $F = 12.66$, $P > 0.9999$; $F = 11.21$, $P = 0.8088$).

Recent studies have shown that activated microglia produce ROS and cause neuronal damage (Liu et al., 2023). To determine whether Gyp-XLIX can mitigate oxidative stress, ROS in the mouse cerebral cortex were stained with DHE. Compared with the Sham group, the CLP group

presented noticeably higher ROS levels ($F = 174.1$, $P < 0.0001$). On the other hand, the CLP mice treated with Gyp-XLIX presented decreased ROS levels ($F = 174.1$, $P < 0.0001$). Compared with the CLP + DEX group, the CLP + Gyp-XLIX group presented no significant difference in ROS levels ($F = 174.1$, $P = 0.5027$), suggesting that Gyp-XLIX has the same ability to relieve ROS as DEX does (Fig. 4E–F). Compared with Sham mice, CLP mice presented higher levels of Keap1 ($F = 11.84$, $P = 0.0106$) and lower expression of Nrf2 ($F = 11.09$, $P = 0.0127$), and the

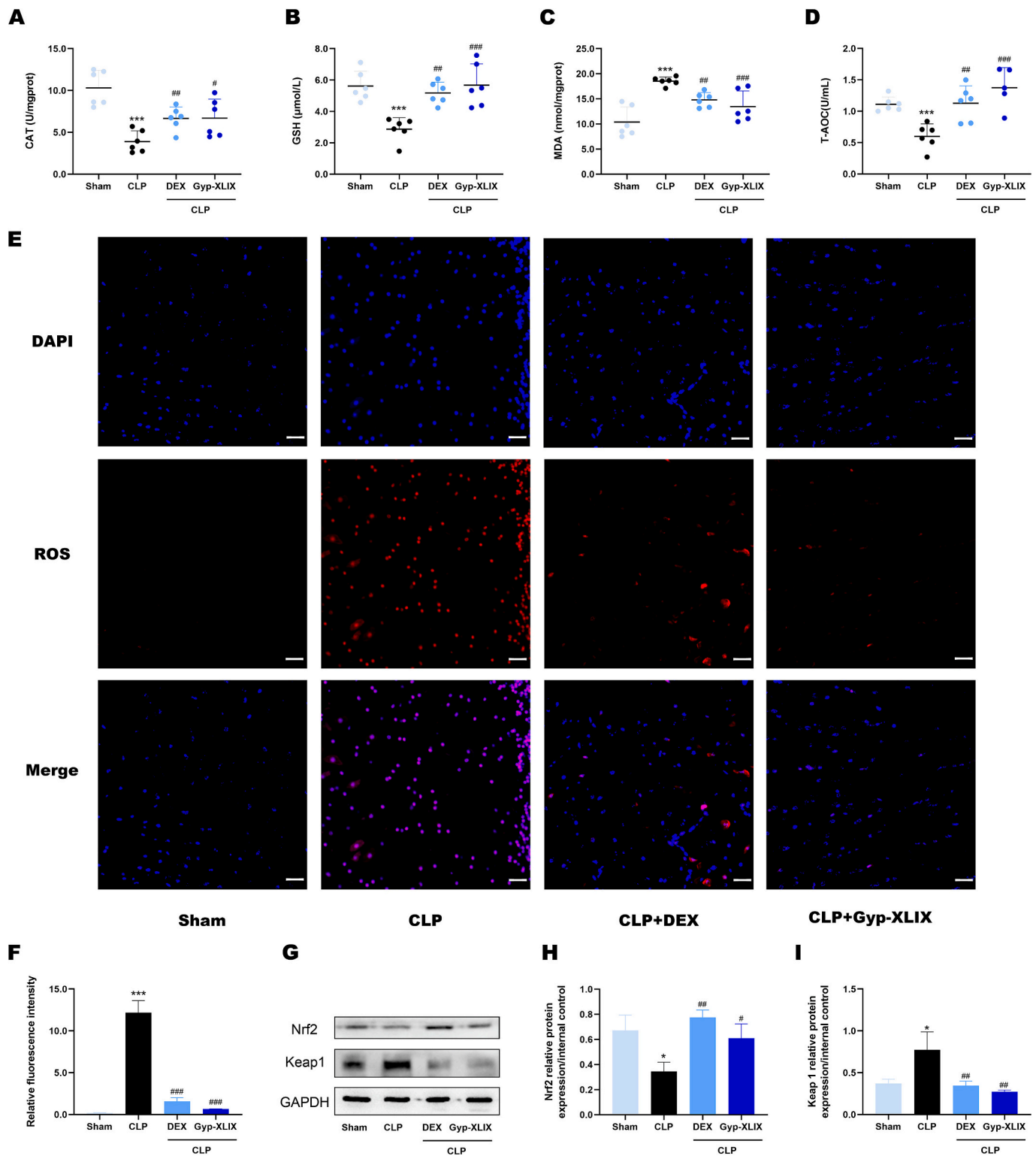


Fig. 4. Gypenoside XLIX improves oxidative stress during SAE. (A–D) The CAT activity, GSH content, MDA content, and T-AOC activity in each group were evaluated using supernatant from brain tissue homogenate, $n = 6$. (E) Cortical ROS staining of brain tissue. Red signal: ROS was generated, and the ROS fluorescence intensity was quantified (F). Scale bar = 100 μm , $n = 3$. (G) The expression levels of Keap 1 and Nrf2 important proteins were measured and normalized using proteins isolated from brain tissue, with GAPDH as an internal control, $n = 3$. (For interpretation of the references to colour in this figure legend, the reader is referred to the web version of this article.)

results revealed that the level of oxidative stress in the brain tissue of CLP mice was increased. After treatment with Gyp-XLIX, the changes in the expression of these proteins were reversed, as reflected by decreases in Keap1 expression ($F = 11.84$, $P = 0.0029$) and increases in Nrf2

expression ($F = 11.09$, $P = 0.0377$). This result was not significantly different from that of the CLP + DEX group ($F = 11.84$, $P = 0.8720$; $F = 11.09$, $P = 0.2279$), indicating that Gyp-XLIX and DEX played the same role in preventing oxidative stress (Fig. 4G–I). These results suggest that

Gyp-XLIX improves oxidative stress during SAE by activating the cellular protective system associated with Nrf2.

3.5. Gyp-XLIX treatment inhibited cell apoptosis during SAE

An increase in apoptosis is related to the pathogenesis of SAE (Chen et al., 2020). In brief, compared with Sham group, tunel staining of a large number of cortical cells in CLP group showed red signal (showed by red triangle symbol), indicating that CLP process was accompanied by apoptosis of brain cells. In addition, both Gyp-XLIX and DEX can reduce the red signal, indicating that Gyp-XLIX and DEX can effectively reduce the apoptosis of brain cells induced by CLP. However, GW6471 reversed the anti-apoptotic effect of Gyp-XLIX on the cerebral cortex of CLP mice (Fig. 5A). In addition, we detected the expression of apoptosis-related proteins. Compared with the Sham group, CLP significantly increased the expression levels of Bax ($F = 20.47$, $P = 0.0055$) and Cyto-C ($F = 29.15$, $P = 0.0003$) and inhibited the expression of Bcl-2 ($F = 8.066$, $P = 0.0092$). In contrast, Gyp-XLIX had a beneficial effect by reversing these changes in protein expression in CLP-treated mice, downregulating the protein levels of Bax ($F = 20.47$, $P = 0.0007$) and Cyto-C ($F = 29.15$, $P = 0.0002$), and increasing the protein levels of Bcl-2 ($F = 8.066$, $P = 0.0425$). In contrast, compared with those of CLP + DEX, the expression of these proteins was not significantly different ($F = 20.47$, $P = 0.9979$; $F = 29.15$, $P = 0.7540$; $F = 8.066$, $P = 0.9189$), indicating that the antiapoptotic ability of Gyp-XLIX was not significantly different from that of DEX (Fig. 5B-E). These results suggest that the administration of Gyp-XLIX alleviates SAE-induced apoptosis.

3.6. Gyp-XLIX plays a role in alleviating SAE by activating PPAR- α and acting on its downstream MAPK signalling pathway

To investigate the mechanism of SAE in more detail, we used the GEO database to conduct a more in-depth study. We discovered that the expression of PPAR- α was lower in sepsis patients than in healthy controls ($P < 0.0001$). As shown in Fig. 6A, PPAR- α seems to be crucial in the development of SAE, and a decrease in its expression was directly

linked to the onset of SAE.

This result was further verified by western blotting detection of PPAR- α protein expression levels in each group of mice. Compared with the Sham group, the level of PPAR- α in the CLP group was lower ($F = 6.705$, $P = 0.0432$). However, after Gyp-XLIX administration, the protein expression of PPAR- α was significantly greater than that in the CLP group ($F = 6.705$, $P = 0.0450$). Moreover, the downstream MAPK signalling pathway was activated in SAE after the reduction in PPAR- α ($F = 9.792$, $P = 0.0138$; $F = 15.25$, $P = 0.0076$), and the activation of MAPK was also alleviated after treatment with Gyp-XLIX ($F = 9.792$, $P = 0.0350$; $F = 15.25$, $P = 0.0070$) (Fig. 6B-E). Therefore, we speculated that PPAR- α may be a potential target for the mitigation of SAE by Gyp-XLIX, which plays a role in the mitigation of SAE by activating PPAR- α and acting on its downstream MAPK signalling pathway.

Microglia are central nervous system macrophages and they are essential for neuronal regeneration and healthy brain development. There is increasing evidence that microglia are critical to the pathophysiology of SAE (Michels et al., 2014). Previous studies have shown that in the brain, PPAR- α is expressed in a variety of cell types, including microglia (Marx et al., 2002; Ramanan et al., 2008). To verify whether Gyp-XLIX targets BV-2 cells during SAE, we detected IBA1, a marker of microglial activation. Compared with Sham mice, CLP-treated mice presented increased expression of IBA1 ($F = 16.74$, $P = 0.0037$), which was reduced when Gyp-XLIX was administered ($F = 16.74$, $P = 0.0117$). These results indicate that microglia are overactivated during CLP and that Gyp-XLIX can act on microglia. After Gyp-XLIX treatment, the overactivation of microglia was reduced (Fig. 7A-B). In addition, we used IBA1 to label microglia for colocalization with PPAR- α . Compared with that in the Sham group, the expression of PPAR- α was inhibited in the SAE model group, whereas the fluorescence signal of PPAR- α was restored by Gyp-XLIX intervention (Fig. 7C). We also examined the colocalization of PPAR- α with astrocytes and neurons, and interestingly, in astrocytes, there was no significant change in PPAR- α expression in the SAE model or Gyp-XLIX intervention. In neurons, PPAR- α expression was inhibited in the SAE model group compared with the Sham group, but Gyp-XLIX intervention did not significantly improve PPAR- α

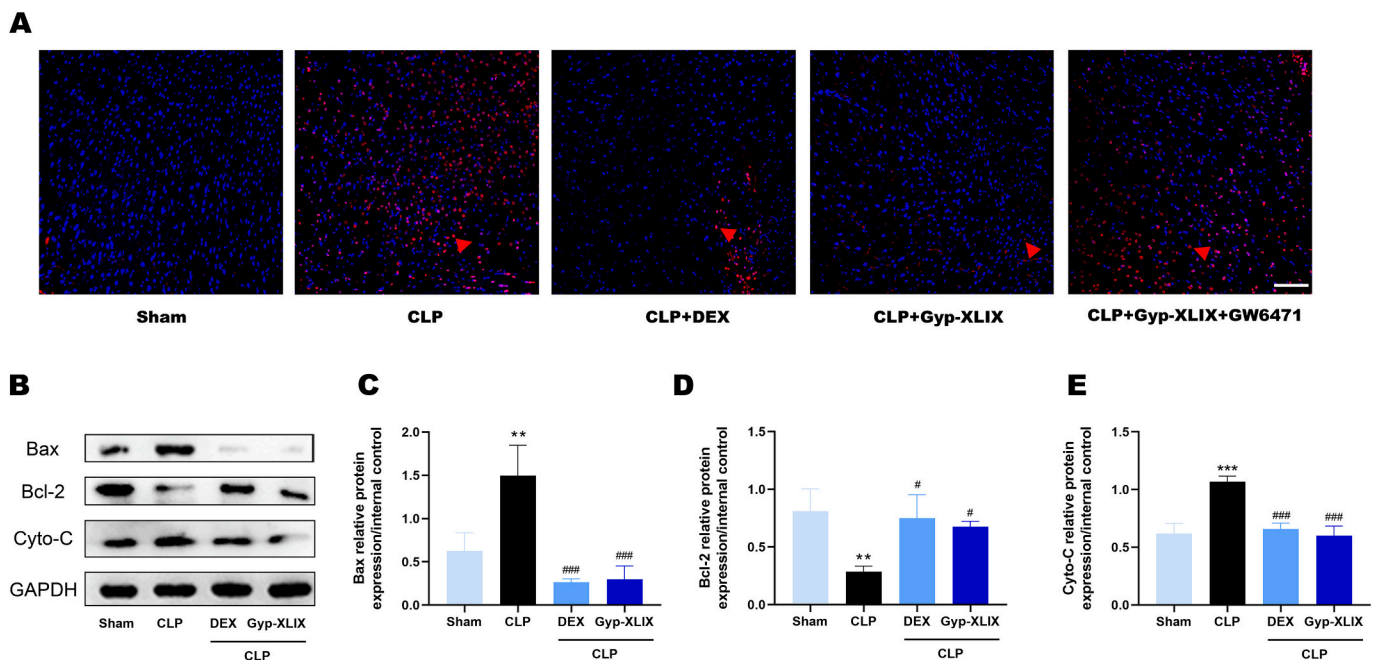


Fig. 5. Gypenoside XLIX treatment inhibited apoptosis during SAE. (A) Observation of the brain cortex cells apoptosis by tunnel staining, the red signals represent apoptotic cells. Scale bar = 100 μ m. (B-E) In order to evaluate the expression of apoptosis-related proteins Bax, Bcl-2 and cytochrome C, protein extracts from brain tissue were extracted and homogenized, and GAPDH was used as an internal control, $n = 3$. (For interpretation of the references to colour in this figure legend, the reader is referred to the web version of this article.)

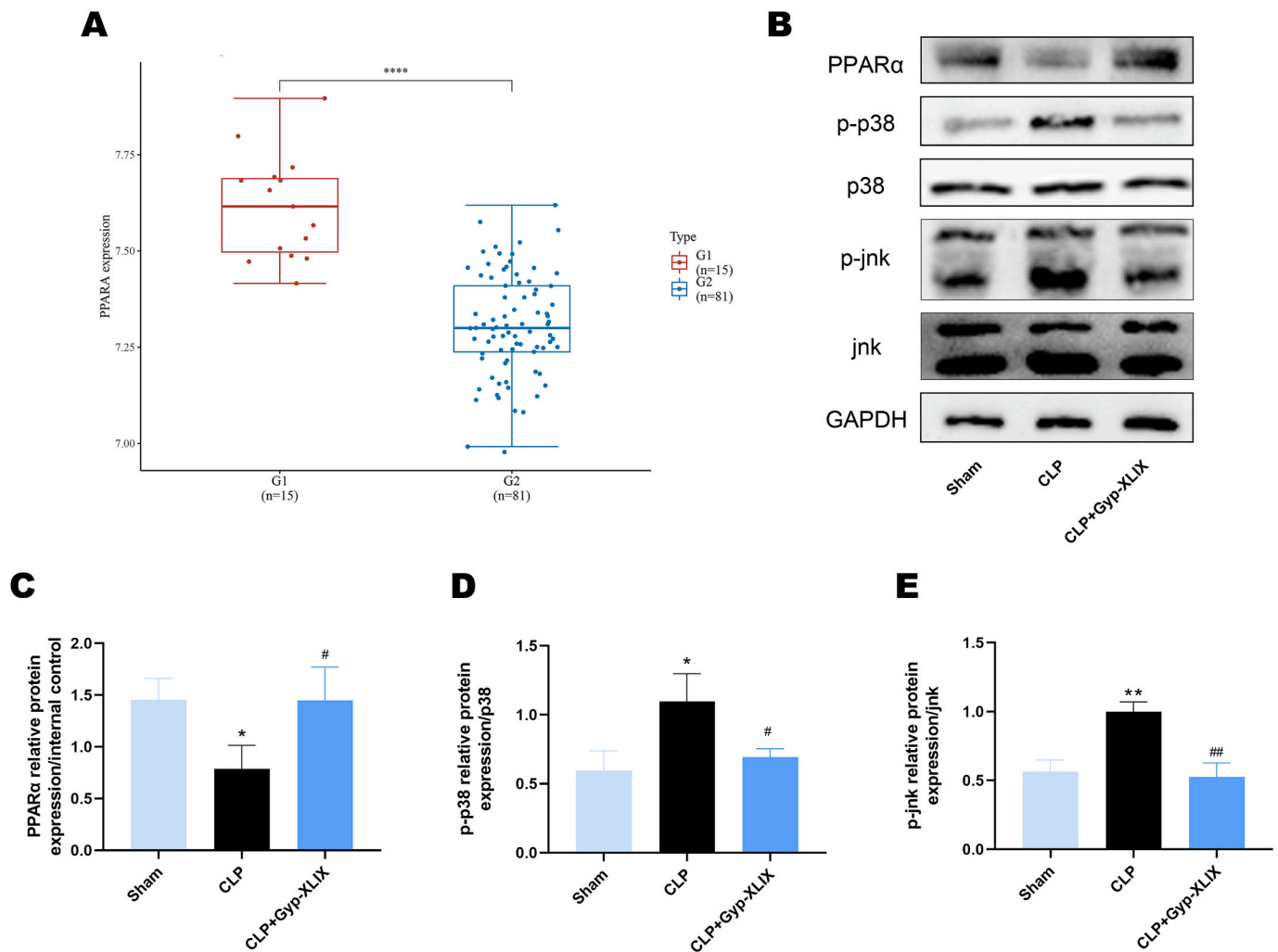


Fig. 6. Gypenoside XLIX can increase the expression of PPAR- α . (A) The mRNA expression levels of PPAR- α in patients with sepsis and patients without sepsis were analyzed using GEO database, where G1 represented the group of patients without sepsis and G2 represented the group of patients with sepsis. (B–E) Expression levels of PPAR- α , p-p38, p38, p-jnk and jnk proteins were measured and homogenized using proteins isolated from brain tissue, with GAPDH as the internal reference, $n = 3$.

expression, which may be related to neuron damage (Fig. S2). We subsequently used BV-2 cells in subsequent in vitro experiments. Thus, to mimic SAE, we stimulated BV-2 cells with LPS. First, we investigated the impact of Gyp-XLIX on BV-2 activity via a CCK8 assay. We discovered that BV-2 cells were toxically affected by 20 μ M Gyp-XLIX (Fig. 7D). Therefore, in the follow-up study, we used a 10 μ M concentration to conduct the experiment.

To further determine whether the role of Gyp-XLIX in SAE is related to PPAR- α , we used GW6471 for validation. Next, we examined the effect on NO in each group. Compared with that in the normal group, the NO content increased after LPS treatment ($F = 21.88$, $P = 0.0011$), whereas the NO content decreased in the LPS + Gyp-XLIX treatment group ($F = 21.88$, $P = 0.0012$); however, the PPAR- α inhibitor GW6471 partially counteracted this effect ($F = 21.88$, $P = 0.0042$). (Fig. 7E). Moreover, FSC detection of the ROS content also revealed the same effect, and ROS were restored in cells incubated with Gyp-XLIX. GW6471 eliminated the effective effect of Gyp-XLIX (Fig. 7F). In addition, WB experiments showed that PPAR- α expression was downregulated in vivo and in vitro after injury. Compared with that in the control group, the PPAR- α protein level decreased after LPS stimulation ($F = 39.74$, $P < 0.0001$), and Gyp-XLIX administration increased PPAR- α expression ($F = 39.74$, $P = 0.0008$); however, the use of PPAR- α inhibitors partially reversed this effect ($F = 39.74$, $P = 0.0024$). Moreover, compared with

that in the control group, the expression of MAPK-related proteins increased with LPS stimulation ($F = 30.30$, $P = 0.0198$; $F = 14.75$, $P = 0.0019$) and was effectively reduced after Gyp-XLIX treatment ($F = 30.30$, $P = 0.0028$; $F = 14.75$, $P = 0.0097$). Moreover, the expression of MAPK signalling pathway proteins in the middle and downstream regions of each group also increased after GW6471 intervention ($F = 30.30$, $P = 0.0001$; $F = 14.75$, $P = 0.0416$), which was closely related to the expression of PPAR- α . These results indicated that PPAR- α expression decreased after LPS stimulation, but Gyp-XLIX activated PPAR- α expression (Fig. 7G–J). Similarly, the detection of proteins related to inflammation, oxidative stress and apoptosis also showed the same results as those of the in vivo studies (Fig. 7K–T). GW6471 reversed the therapeutic effect of Gyp-XLIX on LPS, indicating that during SAE, Gyp-XLIX improved inflammation, oxidative stress and apoptosis, which are PPAR- α targets. Therefore, we suggest that Gyp-XLIX can alleviate the LPS-induced decrease in PPAR- α and regulate the MAPK signalling pathway to relieve inflammation, oxidative stress, and apoptosis in brain tissue to treat SAE. (See Fig. 8.)

4. Discussion

Since ancient times, sepsis has been thought to impact the central nervous system (CNS), with so-called sepsis-associated encephalopathy

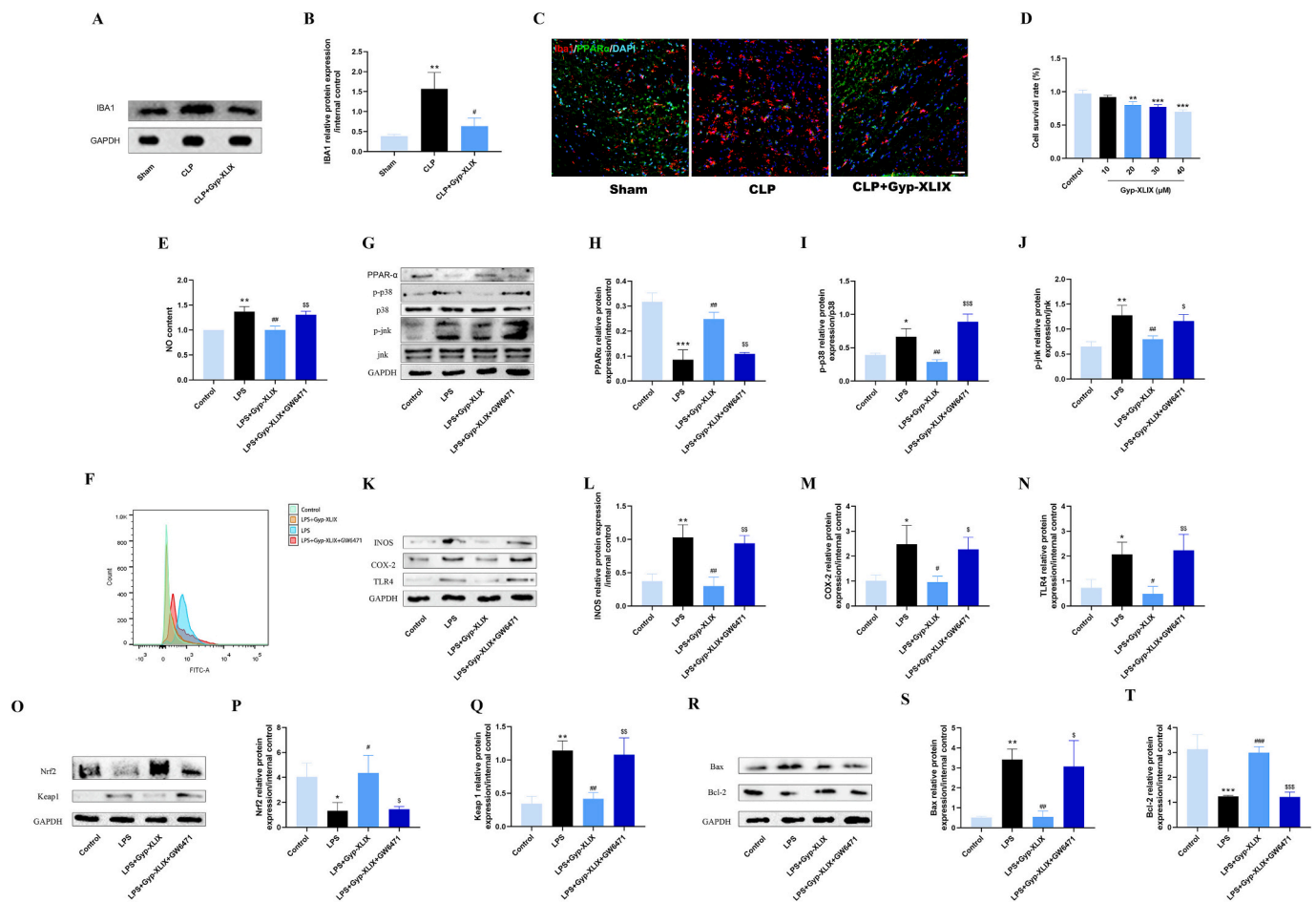


Fig. 7. Gypenoside XLIX plays a role in alleviating SAE by activating PPAR- α and acting on its downstream MAPK signalling pathway. The SAE model was established in vitro by stimulating BV-2 cells with 1 μ g/mL LPS. (A–B) the expression of IBA1 in brain tissues of mice in each group was detected. With GAPDH as the internal reference, $n = 3$. (C) PPAR- α and IBA1 colocalization fluorescence map. Scale bar = 50 μ m. (D) The effect of gypenoside XLIX at different concentrations (10, 20, 30, 40 μ M) on BV-2 was detected by CCK8, $n = 6$. (E) Measurement of NO in cells of different treatment groups, $n = 6$. (F) The expression of ROS in each group was measured by flow cytometry, with green representing the control group, orange representing the LPS + gypenoside XLIX administration group, blue representing the LPS stimulation group, and red representing the LPS + gypenoside XLIX + GW6471 group, $n = 3$. (G–J) was validated in vitro to detect PPAR- α and MAPK signalling pathways in each group of BV-2 cells. (K–N) The inflammatory related proteins in BV-2, iNOS, COX-2, TLR4, were detected and homogenized in each group, with GAPDH as the internal reference, $n = 3$. (O–Q) The oxidative stress-related proteins Nrf2 and Keap1 in BV-2 of each group were detected and homogenized, with GAPDH as the internal reference, $n = 3$. (P–T) The apoptosis-related proteins in BV-2 were detected and homogenized in each group: Bax, Bcl-2, GAPDH as internal reference, $n = 3$. (For interpretation of the references to colour in this figure legend, the reader is referred to the web version of this article.)

serving as its clinical manifestation (Mazeraud et al., 2020), which leads to worsening sepsis and high mortality (Wu et al., 2021), and SAE can cause behavioural symptoms that range from coma to dementia. New SAE treatment approaches will benefit from an understanding of the underlying causes (Barichello et al., 2021). Numerous studies on SAE have been conducted in recent decades, but its precise mechanism is still unclear (Zhu et al., 2023). At present, various therapeutic strategies, such as the use of activated protein C and steroids, have been attempted in SAE models (Chaudhry and Duggal, 2014); however, an appropriate treatment for SAE is lacking.

We investigated the possible therapeutic benefit of Gyp-XLIX in SAE in this study. According to our results, Gyp-XLIX effectively alleviates a series of phenomena, such as CLP-induced increases in mortality, cerebral nerve defects, BBB destruction, and cerebral neuroinflammation. These effects are caused mainly by the activation of the PPAR- α pathway. Therefore, our findings demonstrate that Gyp-XLIX may be a neuroprotective agent for SAE and has strong therapeutic potential for SAE.

Previous studies have suggested that acute brain nerve injury is largely reversible with appropriate treatment (Chaudhry and Duggal, 2014). To verify whether Gyp-XLIX can reverse SAE injury, we first

monitored mortality, body weight, the brain defect score and other indicators and found that after Gyp-XLIX treatment, SAE mice experienced obvious improvements. Dexamethasone has the same therapeutic effect. Reports indicate that atrophy of the hippocampus and cortex may be connected to sepsis accompanied by aberrant neurological symptoms (Stubbs et al., 2013). We used HE to assess the condition of the cortex and hippocampus and found that the brain damage induced by CLP could be reversed by Gyp-XLIX, which indicated that Gyp-XLIX had an initial protective effect.

An increasing amount of research on humans and animal models suggests that SAE is linked to numerous long-term cognitive consequences (Rothenhäusler et al., 2001). It is believed that cognitive impairment is caused by hippocampal damage associated with early sepsis (Semmler et al., 2013). HE staining revealed that significant hippocampal damage could be alleviated by the administration of Gyp-XLIX. Consequently, we hypothesized that Gyp-XLIX may reduce SAE-induced cognitive impairment in mice. Cognitive tests with an elevated cross maze and a maze showed that Gyp-XLIX can improve cognitive impairment in SAE mice.

According to previous reports, alterations in the permeability of the blood–brain barrier during sepsis generate a number of clinical and

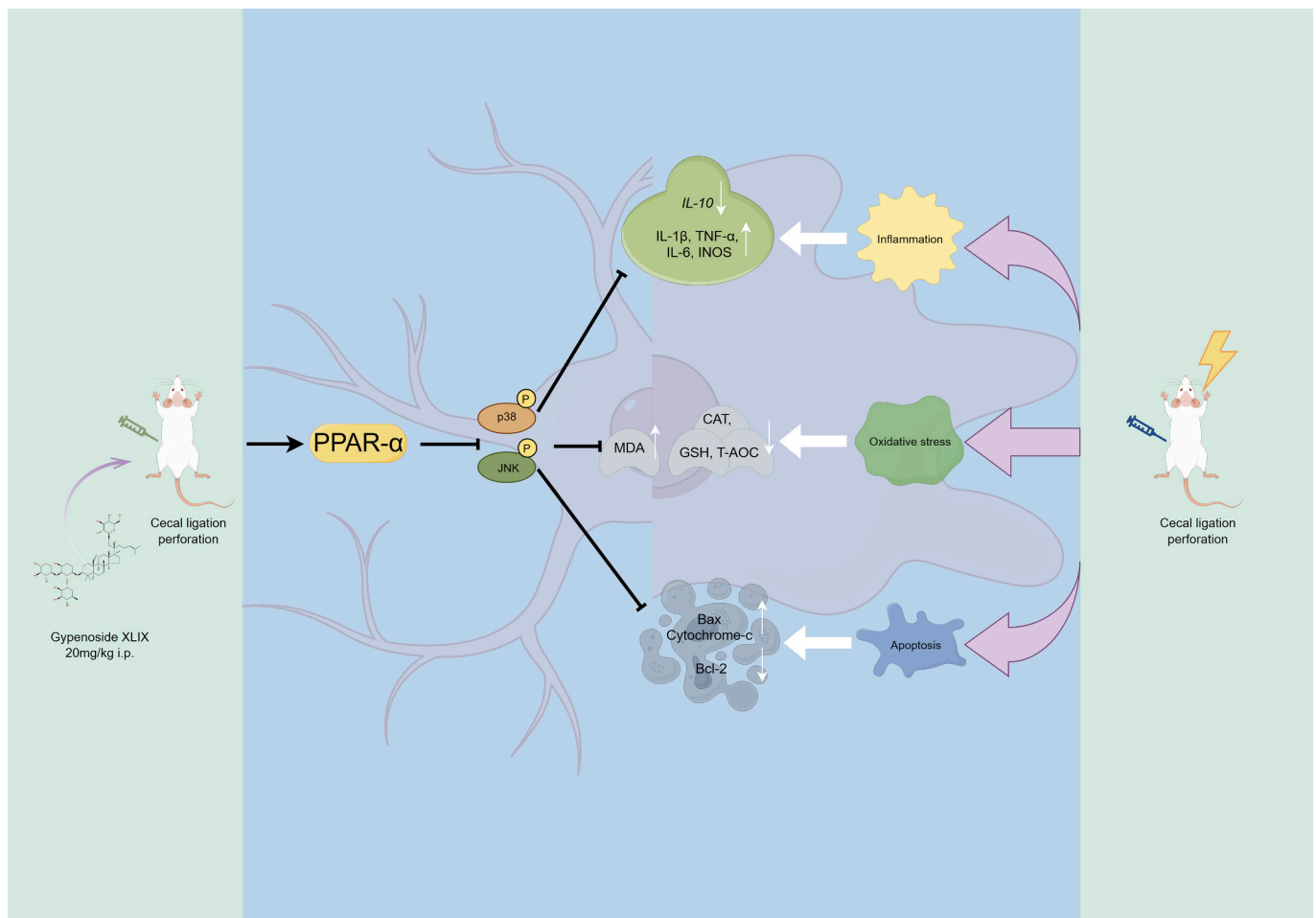


Fig. 8. Gypenoside XLIX acts on microglia and then targets PPAR- α and downstream p38 MAPK. JNK MAPK regulates inflammation, oxidative stress and apoptosis during SAE, thus playing a therapeutic role.

functional changes in brain tissue, including oedema (You and Jiang, 2021), in addition to a higher concentration of water in the brain and a greater susceptibility to blood dyes. Consistent with earlier findings, we observed increased brain oedema and BBB permeability following CLP in this study. However, after treatment with Gyp-XLIX, the increase in cerebral oedema and increased blood–brain barrier permeability were significantly reversed, suggesting that the damage to the blood–brain barrier during SAE can also be reversed by Gyp-XLIX.

The primary pathophysiological mechanisms linked to the development of SAE are neuroinflammation, oxidative stress, and cell death (Peng et al., 2021; Zhang et al., 2021a). Normally, the BBB allows only trace levels of inflammatory agents, including TNF- α , IL-1, and IL-6, to reach the brain. On the other hand, when systemic inflammation occurs, the BBB is destroyed, which makes it possible for infections, neurotoxins, complement, and a variety of inflammatory cytokines to reach the brain tissue (Ren et al., 2020); thus, we also examined neuroinflammation and oxidative stress. Previous animal sepsis models have shown markedly elevated brain tissue expression levels of inflammatory markers such as TNF- α , IL-1, and IL-6. In line with earlier findings, we discovered that there was a notable increase in the expression of inflammatory markers, suggesting that inflammation followed the SAE process when the BBB was destroyed. Interestingly, this phenomenon can be improved by the administration of Gyp-XLIX, indicating that Gyp-XLIX effectively alleviates the inflammatory response in SAE. Similarly, oxidative stress can cause neuronal damage and brain dysfunction during sepsis (Barichello et al., 2006), and excessive ROS production can induce lipid peroxidation, which damages cell and mitochondrial

membranes. Lipid peroxidation directly results in the production of MDA, which is considered an indicator of ROS-mediated damage. GSH and CAT are two important antioxidant enzymes that scavenge ROS (Zhang et al., 2021a). To evaluate the degree of oxidative damage in the brain tissue in each group of mice, we detected the levels of ROS in the cerebral cortex and hippocampus, in addition to the related enzymes and ROS, and found that the oxidative damage caused by SAE improved after the administration of Gyp-XLIX. One type of noninflammatory cell death is called apoptosis, and past research has extensively examined how apoptosis affects SAE (Fan et al., 2022). Through tunnel staining, we observed that apoptosis was reduced after the administration of Gyp-XLIX. These findings indicate that Gyp-XLIX has anti-inflammatory, antioxidant and antiapoptotic effects on CLP-induced cerebral neuronal injury in septic mice.

The role of the signal transduction system in the aetiology and progression of SAE has garnered increasing attention in recent years (Yu et al., 2019). The brain and other organs express PPAR- α and other receptors in this family, which can be implicated in the transcriptional regulation of genes linked to neuroinflammation, neuroapoptosis, and antioxidant defence (Corbett et al., 2015; Dutta et al., 2022). In addition, PPAR- α promotes neurogenesis and cell differentiation in the CNS and has been shown to have protective effects in neuroinflammatory lesions. Research has indicated that particular PPAR- α activators could be crucial in ameliorating neuro-related illnesses (Wójtowicz et al., 2020), and the most promising treatment approach for neuro-related illnesses is thought to include activating PPAR- α . Notably, PPAR- α agonists function as neuroprotective drugs in a range of neurological conditions,

including multiple sclerosis, cerebral ischaemia, Parkinson's disease, and Alzheimer's disease (Nisbett and Pinna, 2018). One of the most evident examples is the reduction in antioxidant and anti-inflammatory processes in Alzheimer's disease patients' brains due to the down-regulation of PPAR- α , which can also alter fatty acid transport, lipid metabolism, and mitochondrial dysfunction (Wójtowicz et al., 2020). Moreover, activating PPAR- α has been shown in investigations of Alzheimer's disease to lessen Alzheimer-like pathology and cognitive impairment in animal models of the disease (Luo et al., 2020).

Thus, we hypothesized that PPAR- α might be important for the development of SAE. We verified that the level of PPAR- α tended to decrease in sepsis patients through analysis of the GEO database, suggesting that PPAR- α may be associated with injury. However, when we treated cells with Gyp-XLIX to ameliorate the decrease in PPAR- α while alleviating SAE damage, the same effect was observed at the cellular level, and our results demonstrated that PPAR- α may be the target through which Gyp-XLIX regulates the pathophysiological function of SAE. Inflammation, oxidative stress, and apoptosis can be new targets for treating SAE injury.

In summary, the activation of PPAR- α may be a potential target for the treatment of SAE, and it is also a key mechanism by which Gyp-XLIX exerts its anti-inflammatory, oxidative stress, and apoptotic effects, which provides new insights for the clinical treatment of SAE patients.

Supplementary data to this article can be found online at <https://doi.org/10.1016/j.expneurol.2024.115027>.

Funding

This work was supported by the following grants: the National Natural Science Foundation of China (No. 82402658), the Lianyungang Science and Technology Program (Project No. 23JCYJ015), the Lianyungang Aging Health Research Project (Project No. L202301), and the Lianyungang First People's Hospital Doctoral Research Start-up Fund (Project No. BS202314). The funders had no role in study design, data collection and analysis, decision to publish, or preparation of the manuscript.

Ethics

All mice were housed in a dedicated pathogen-free facility, and all animal experiments were conducted following protocols approved by the Institutional Animal Ethics Committee of Jiangsu Ocean University.

CRediT authorship contribution statement

Panpan Zhao: Writing – review & editing, Formal analysis, Conceptualization. **Wei Zhang:** Writing – original draft, Data curation, Conceptualization. **Xinyu Zhou:** Software, Formal analysis. **Yikun Zhao:** Methodology, Investigation. **Aimin Li:** Supervision, Project administration. **Yong Sun:** Supervision, Resources.

Declaration of competing interest

The authors declare that they have no known competing financial interests or personal relationships that could have appeared to influence the work reported in this paper.

Acknowledgements

The author is grateful to the National Natural Science Foundation of China (No. 82402658), the Jiangsu Science and Technology Project (No. BK20240492), Lianyungang Science and Technology Program (Project No. 23JCYJ015), Lianyungang Aging Health Research Project (Project No. L202301), and also to Lianyungang First People's Hospital Doctoral Research Start-up Fund (Project No. BS202314).

Data availability

The datasets used and/or analyzed during the current study are available from the corresponding author on reasonable request.

References

- Barichello, T., Fortunato, J.J., Vitali, A.M., Feier, G., Reinke, A., Moreira, J.C., Quevedo, J., Dal-Pizzol, F., 2006. Oxidative variables in the rat brain after sepsis induced by cecal ligation and perforation. *Crit. Care Med.* 34, 886–889.
- Barichello, T., Generoso, J.S., Collodel, A., Petronilho, F., Dal-Pizzol, F., 2021. The blood-brain barrier dysfunction in sepsis. *Tissue barriers* 9, 1840912.
- Barrett, T., Wilhite, S.E., Ledoux, P., Evangelista, C., Kim, I.F., Tomashevsky, M., Marshall, K.A., Phillippy, K.H., Sherman, P.M., Holko, M., Yefanov, A., Lee, H., Zhang, N., Robertson, C.L., Serova, N., Davis, S., Soboleva, A., 2013. NCBI GEO: archive for functional genomics data sets—update. *Nucleic Acids Res.* 41, D991–D995.
- Caillaud, M., Patel, N.H., White, A., Wood, M., Contreras, K.M., Toma, W., Alkhlaif, Y., Roberts, J.L., Tran, T.H., Jackson, A.B., Poklis, J., Gewirtz, D.A., Damaj, M.I., 2021. Targeting peroxisome proliferator-activated receptor- α (PPAR- α) to reduce paclitaxel-induced peripheral neuropathy. *Brain Behav. Immun.* 93, 172–185.
- Cassol Jr., O.J., Comim, C.M., Petronilho, F., Constantino, L.S., Streck, E.L., Quevedo, J., Dal-Pizzol, F., 2010. Low dose dexamethasone reverses depressive-like parameters and memory impairment in rats submitted to sepsis. *Neurosci. Lett.* 473, 126–130.
- Chaudhry, N., Duggal, A.K., 2014. Sepsis Associated Encephalopathy. *Advances in Medicine* 2014, 762320.
- Chen, S., Tang, C., Ding, H., Wang, Z., Liu, X., Chai, Y., Jiang, W., Han, Y., Zeng, H., 2020. Maf1 ameliorates Sepsis-associated encephalopathy by suppressing the NF- κ B/NLRP3 inflammasome signaling pathway. *Front. Immunol.* 11, 594071.
- Corbett, G.T., Gonzalez, F.J., Pahan, K., 2015. Activation of peroxisome proliferator-activated receptor α stimulates ADAM10-mediated proteolysis of APP. *Proc. Natl. Acad. Sci. U. S. A.* 112, 8445–8450.
- Ding, H., Li, Y., Chen, S., Wen, Y., Zhang, S., Luo, E., Li, X., Zhong, W., Zeng, H., 2022. Fisetin ameliorates cognitive impairment by activating mitophagy and suppressing neuroinflammation in rats with sepsis-associated encephalopathy. *CNS Neurosci. Ther.* 28, 247–258.
- Dong, L., Yang, K.Q., Fu, W.Y., Shang, Z.H., Zhang, Q.Y., Jing, F.M., Li, L.L., Xin, H., Wang, X.J., 2014. Gypenosides protected the neural stem cells in the subventricular zone of neonatal rats that were prenatally exposed to ethanol. *Int. J. Mol. Sci.* 15, 21967–21979.
- Dong, S.Q., Zhang, Q.P., Zhu, J.X., Chen, M., Li, C.F., Liu, Q., Geng, D., Yi, L.T., 2018. Gypenosides reverses depressive behavior via inhibiting hippocampal neuroinflammation. *Biomedicine & pharmacotherapy = Biomedecine & pharmacotherapie* 106, 1153–1160.
- Dutta, D., Paidi, R.K., Raha, S., Roy, A., Chandra, S., Pahan, K., 2022. Treadmill exercise reduces α -synuclein spreading via PPAR α . *Cell Rep.* 40, 111058.
- Esmaili, M.A., Yadav, S., Gupta, R.K., Waggoner, G.R., Deloach, A., Calingasan, N.Y., Beal, M.F., Kiaei, M., 2016. Preferential PPAR- α activation reduces neuroinflammation, and blocks neurodegeneration in vivo. *Hum. Mol. Genet.* 25, 317–327.
- Fan, Z., Ma, H., Li, Y., Wu, Y., Wang, J., Xiong, L., Fang, Z., Zhang, X., 2022. Neuronal MD2 induces long-term mental impairments in septic mice by facilitating necroptosis and apoptosis. *Front. Pharmacol.* 13, 884821.
- Gao, L.L., Wang, Z.H., Mu, Y.H., Liu, Z.L., Pang, L., 2022. Emodin promotes autophagy and prevents apoptosis in Sepsis-associated encephalopathy through activating BDNF/TrkB signaling. *Pathobiology : Journal of Immunopathology, Molecular and Cellular Biology* 89, 135–145.
- Guo, S., Sui, C., Ma, Y., 2017. Development of a targeted method for quantification of gypenoside XLIX in rat plasma, using SPE and LC-MS/MS. *Biomedical Chromatography : BMC* 31.
- Guo, P., Jin, Z., Wu, H., Li, X., Ke, J., Zhang, Z., Zhao, Q., 2019. Effects of irisin on the dysfunction of blood-brain barrier in rats after focal cerebral ischemia/reperfusion. *Brain and Behavior* 9, e01425.
- Huang, T.H., Tran, V.H., Roufogalis, B.D., Li, Y., 2007. Gypenoside XLIX, a naturally occurring PPAR-alpha activator, inhibits cytokine-induced vascular cell adhesion molecule-1 expression and activity in human endothelial cells. *Eur. J. Pharmacol.* 565, 158–165.
- Kumar, S., Tripathy, S., Jyoti, A., Singh, S.G., 2019. Recent advances in biosensors for diagnosis and detection of sepsis: a comprehensive review. *Biosens. Bioelectron.* 124–125, 205–215.
- Lee, H.L., Kim, J.M., Go, M.J., Lee, H.S., Kim, J.H., Heo, H.J., 2024. Fermented *Protaetia brevitarsis* Larvae Improves Neurotoxicity in Chronic Ethanol-Induced-Dementia Mice via Suppressing AKT and NF- κ B Signaling Pathway, 25, p. 2629.
- Li, H., Liao, H., Zhang, C., Xu, Y., Xu, X., Chen, Y., Song, S., Li, Q., Si, Y., Bao, H., 2022. Disrupted metabolic and spontaneous neuronal activity of hippocampus in sepsis associated encephalopathy rats: a study combining magnetic resonance spectroscopy and resting-state functional magnetic resonance imaging. *Front. Neurosci.* 16, 1032098.
- Li, N., Ma, R.H., Zhang, E.F., Ge, F., Fang, D.Y., Zhang, J., Zhang, Y.N., Gao, Y., Hou, L.C., Jin, H.X., 2023. Interferon-induced transmembrane protein 3 in the hippocampus: a potential novel target for the therapeutic effects of recombinant human brain natriuretic peptide on sepsis-associated encephalopathy. *Front. Mol. Neurosci.* 16, 1182005.

- Liu, Y., Yang, H., Luo, N., Fu, Y., Qiu, F., Pan, Z., Li, X., Jian, W., Yang, X., Xue, Q., Luo, Y., Yu, B., Liu, Z., 2023. An Fgr kinase inhibitor attenuates sepsis-associated encephalopathy by ameliorating mitochondrial dysfunction, oxidative stress, and neuroinflammation via the SIRT1/PGC-1 α signaling pathway. *J. Transl. Med.* 21, 486.
- Luo, R., Su, L.Y., Li, G., Yang, J., Liu, Q., Yang, L.X., Zhang, D.F., Zhou, H., Xu, M., Fan, Y., Li, J., Yao, Y.G., 2020. Activation of PPARA-mediated autophagy reduces Alzheimer disease-like pathology and cognitive decline in a murine model. *Autophagy* 16, 52–69.
- Marx, N., Kehrle, B., Kohlhammer, K., Grüb, M., Koenig, W., Hombach, V., Libby, P., Plutzky, J., 2002. PPAR activators as antiinflammatory mediators in human T lymphocytes: implications for atherosclerosis and transplantation-associated arteriosclerosis. *Circ. Res.* 90, 703–710.
- Mazeraud, A., Righy, C., Bouchereau, E., Benghanem, S., Bozza, F.A., Sharshar, T., 2020. Septic-associated encephalopathy: a comprehensive review. *Neurotherapeutics: the Journal of the American Society for Experimental NeuroTherapeutics* 17, 392–403.
- Mei, B., Li, J., Zuo, Z., 2021. Dexmedetomidine attenuates sepsis-associated inflammation and encephalopathy via central α 2A adrenoceptor. *Brain Behav. Immun.* 91, 296–314.
- Meneses, G., Cárdenas, G., Espinosa, A., Rassy, D., Pérez-Osorio, I.N., Bárcena, B., Fleury, A., Besedovsky, H., Fragos, G., Sciutto, E., 2019. Sepsis: developing new alternatives to reduce neuroinflammation and attenuate brain injury. *Ann. N. Y. Acad. Sci.* 1437, 43–56.
- Michels, M., Danielski, L.G., Dal-Pizzol, F., Petronilho, F., 2014. Neuroinflammation: microglial activation during sepsis. *Curr. Neurovasc. Res.* 11, 262–270.
- Nisbett, K.E., Pinna, G., 2018. Emerging therapeutic role of PPAR- α in cognition and emotions. *Front. Pharmacol.* 9, 998.
- Oliveira, A.C., Bertollo, C.M., Rocha, L.T., Nascimento Jr., E.B., Costa, K.A., Coelho, M. M., 2007. Antinociceptive and antiedematogenic activities of fenofibrate, an agonist of PPAR alpha, and pioglitazone, an agonist of PPAR gamma. *Eur. J. Pharmacol.* 561, 194–201.
- Pan, S., Lv, Z., Wang, R., Shu, H., Yuan, S., Yu, Y., Shang, Y., 2022. Sepsis-induced brain dysfunction: pathogenesis, diagnosis, and treatment. *Oxidative Med. Cell. Longev.* 2022, 1328729.
- Peng, X., Luo, Z., He, S., Zhang, L., Li, Y., 2021. Blood-brain barrier disruption by lipopolysaccharide and Sepsis-associated encephalopathy. *Front. Cell. Infect. Microbiol.* 11, 768108.
- Pu, Y., Zhao, L., Xi, Y., Xia, Y., Qian, Y., 2022. The protective effects of mirtazapine against lipopolysaccharide (LPS)-induced brain vascular hyperpermeability. *Bioengineered* 13, 3680–3693.
- Ramanan, S., Kooshki, M., Zhao, W., Hsu, F.C., Robbins, M.E., 2008. PPAR α ligands inhibit radiation-induced microglial inflammatory responses by negatively regulating NF- κ B and AP-1 pathways. *Free Radic. Biol. Med.* 45, 1695–1704.
- Reis, L., Oliveira, M.K., Rojas, V.C.T., Batista, T.H., Estevam, E.S., Vitor-Vieira, F., Vilela, F.C., Giusti-Paiva, A., 2022. Curcumin attenuates LPS-induced sickness behavior and fever in rats by modulating Nrf2 activity. *Neurosci. Lett.* 781, 136680.
- Ren, C., Yao, R.Q., Zhang, H., Feng, Y.W., Yao, Y.M., 2020. Sepsis-associated encephalopathy: a vicious cycle of immunosuppression. *J. Neuroinflammation* 17, 14.
- Rothenhäusler, H.B., Ehrentraut, S., Stoll, C., Schelling, G., Kapfhammer, H.P., 2001. The relationship between cognitive performance and employment and health status in long-term survivors of the acute respiratory distress syndrome: results of an exploratory study. *Gen. Hosp. Psychiatry* 23, 90–96.
- Semmler, A., Widmann, C.N., Okulla, T., Urbach, H., Kaiser, M., Widman, G., Mormann, F., Weide, J., Fliessbach, K., Hoef, A., Jessen, F., Putensen, C., Heneka, M.T., 2013. Persistent cognitive impairment, hippocampal atrophy and EEG changes in sepsis survivors. *J. Neurol. Neurosurg. Psychiatry* 84, 62–69.
- Shin, K.S., Zhao, T.T., Choi, H.S., Hwang, B.Y., Lee, C.K., Lee, M.K., 2014. Effects of gypenosides on anxiety disorders in MPTP-lesioned mouse model of Parkinson's disease. *Brain Res.* 1567, 57–65.
- Shin, K.S., Zhao, T.T., Park, K.H., Park, H.J., Hwang, B.Y., Lee, C.K., Lee, M.K., 2015. Gypenosides attenuate the development of L-DOPA-induced dyskinesia in 6-hydroxydopamine-lesioned rat model of Parkinson's disease. *BMC Neurosci.* 16, 23.
- Song, B., Zhou, W., 2022. Amarogentin has protective effects against sepsis-induced brain injury via modulating the AMPK/SIRT1/NF- κ B pathway. *Brain Res. Bull.* 189, 44–56.
- Song, Y.Q., Lin, W.J., Hu, H.J., Wu, S.H., Jing, L., Lu, Q., Zhu, W., 2023. Sodium tanshinone IIA sulfonate attenuates sepsis-associated brain injury via inhibiting NOD-like receptor 3/caspase-1/gasdermin D-mediated pyroptosis. *Int. Immunopharmacol.* 118, 110111.
- Stubbs, D.J., Yamamoto, A.K., Menon, D.K., 2013. Imaging in sepsis-associated encephalopathy—insights and opportunities. *Nat. Rev. Neurol.* 9, 551–561.
- Tang, G., Yang, H., Chen, J., Shi, M., Ge, L., Ge, X., Zhu, G., 2017. Metformin ameliorates sepsis-induced brain injury by inhibiting apoptosis, oxidative stress and neuroinflammation via the PI3K/Akt signaling pathway. *Oncotarget* 8, 97977–97989.
- Wang, P., Niu, L., Gao, L., Li, W.X., Jia, D., Wang, X.L., Gao, G.D., 2010. Neuroprotective effect of gypenosides against oxidative injury in the substantia nigra of a mouse model of Parkinson's disease. *J. Int. Med. Res.* 38, 1084–1092.
- Wang, X.J., Sun, T., Kong, L., Shang, Z.H., Yang, K.Q., Zhang, Q.Y., Jing, F.M., Dong, L., Xu, X.F., Liu, J.X., Xin, H., Chen, Z.Y., 2014. Gypenosides pre-treatment protects the brain against cerebral ischemia and increases neural stem cells/progenitors in the subventricular zone. *International Journal of Developmental Neuroscience: the Official Journal of the International Society for Developmental Neuroscience* 33, 49–56.
- Wen, Q., Ding, Q., Wang, J., Yin, Y., Xu, S., Ju, Y., Ji, H., Liu, B., 2022. Cortistatin-14 exerts neuroprotective effect against microglial activation, blood-brain barrier disruption, and cognitive impairment in Sepsis-associated encephalopathy. *J. Immunol Res* 2022, 3334145.
- Weng, X., Lou, Y.Y., Wang, Y.S., Huang, Y.P., Zhang, J., Yin, Z.Q., Pan, K., 2021. New dammarane-type glycosides from *Gynostemma pentaphyllum* and their lipid-lowering activity. *Bioorg. Chem.* 111, 104843.
- Wójciewicz, S., Strosznajder, A.K., Jeżyna, M., Strosznajder, J.B., 2020. The novel role of PPAR alpha in the brain: promising target in therapy of Alzheimer's disease and other neurodegenerative disorders. *Neurochem. Res.* 45, 972–988.
- Wu, Q., Wang, Y., Li, Q., 2021. Matairesinol exerts anti-inflammatory and antioxidant effects in sepsis-mediated brain injury by repressing the MAPK and NF- κ B pathways through up-regulating AMPK. *Aging* 13, 23780–23795.
- Yamashita, S., Suzuki, T., Iguchi, K., Sakamoto, T., Tomita, K., Yokoo, H., Sakai, M., Misawa, H., Hattori, K., Nagata, T., Watanabe, Y., Matsuda, N., Yoshimura, N., Hattori, Y., 2018. Cardioprotective and functional effects of levosimendan and milrinone in mice with cecal ligation and puncture-induced sepsis. *Naunyn Schmiedeberg's Arch. Pharmacol.* 391, 1021–1032.
- Yin, X.Y., Tang, X.H., Wang, S.X., Zhao, Y.C., Jia, M., Yang, J.J., Ji, M.H., Shen, J.C., 2023. HMGB1 mediates synaptic loss and cognitive impairment in an animal model of sepsis-associated encephalopathy. *J. Neuroinflammation* 20, 69.
- You, L., Jiang, H., 2021. Cabergoline possesses a beneficial effect on blood-brain barrier (BBB) integrity against lipopolysaccharide (LPS). *Bioengineered* 12, 8358–8369.
- Yu, J., Chen, J., Yang, H., Chen, S., Wang, Z., 2019. Overexpression of miR-200a-3p promoted inflammation in sepsis-induced brain injury through ROS-induced NLRP3. *Int. J. Mol. Med.* 44, 1811–1823.
- Zaky, D.A., Eldehna, W.M., El Kerdawy, A.M., Abdallah, D.M., El Abhar, H.S., Wadie, W., 2021. Recombinant human growth hormone improves the immune status of rats with septic encephalopathy: the role of VEGFR2 in the prevalence of endoplasmic reticulum stress repair module. *Int. Immunopharmacol.* 101, 108370.
- Zhang, X., Zhang, W., Jiang, Y., Liu, K., Ran, L., Song, F., 2019. Identification of functional lncRNAs in gastric cancer by integrative analysis of GEO and TCGA data. *J. Cell. Biochem.* 120, 17898–17911.
- Zhang, L., Zhang, X., Wu, T., Pan, X., Wang, Z., 2021a. Isoflurane reduces septic neuron injury by HO-1-mediated abatement of inflammation and apoptosis. *Mol. Med. Rep.* 23.
- Zhang, W., Li, Z., Yang, H., Wang, G., Liu, G., Wang, Y., Bello, B.K., Zhao, P., Liang, W., Dong, J., 2021b. *Aeromonas sobria* induces Proinflammatory cytokines production in mouse macrophages via activating NLRP3 Inflammasome signaling pathways. *Front. Cell. Infect. Microbiol.* 11, 691445.
- Zhang, Y., Chen, Q., Huang, Y., Zhao, R., Sun, J., Yuan, X., Xu, H., Liu, H., Wu, Y., 2021c. Gene excavation and expression analysis of CYP and UGT related to the post modifying stage of gypenoside biosynthesis in *Gynostemma pentaphyllum* (Thunb.) Makino by comprehensive analysis of RNA and proteome sequencing. *PLoS One* 16, e0260027.
- Zhang, W., Chen, H., Xu, Z., Zhang, X., Tan, X., He, N., Shen, J., Dong, J., 2023a. Liensinine pretreatment reduces inflammation, oxidative stress, apoptosis, and autophagy to alleviate sepsis acute kidney injury. *Int. Immunopharmacol.* 122, 110563.
- Zhang, W., Wang, T., Chen, H., Fan, H., Liu, F., Zhang, X., Yang, H., Li, X., Dong, Z., Dong, J., 2023b. Liensinine alleviates septic heart injury by targeting inflammation, oxidative stress, apoptosis, and autophagy. *Acta Biochim. Biophys. Sin.* 55, 521–524.
- Zhang, C., Tian, F., Peng, J., Wang, X., Li, J., Zhang, L., Tan, Z., 2024. Serotonergic neurotransmission mediated cognitive dysfunction in two mouse models of sepsis-associated encephalopathy. *CNS Neurosci. Ther.* 30, e14655.
- Zhao, T.T., Kim, K.S., Shin, K.S., Park, H.J., Kim, H.J., Lee, K.E., Lee, M.K., 2017. Gypenosides ameliorate memory deficits in MPTP-lesioned mouse model of Parkinson's disease treated with L-DOPA. *BMC Complement. Altern. Med.* 17, 449.
- Zhao, H., Jiao, W., Xiu, Y., Zhou, K., Zhong, P., Wang, N., Yu, S., 2022. Enzymatic Biotransformation of Gypenoside XLIX into Gylongiposide I and their Antiviral Roles against Enterovirus 71 in Vitro. *Molecules (Basel, Switzerland)* 27.
- Zhou, G., Fu, X., Wang, L., Cao, Y., Zhuang, J., Hu, J., Li, Y., Xu, C., Gao, S., Shao, A., Wang, L., 2022. Palmitoylethanolamide ameliorates neuroinflammation via modulating PPAR- α to promote the functional outcome after intracerebral hemorrhage. *Neurosci. Lett.* 781, 136648.
- Zhu, C.L., Xie, J., Liu, Q., Wang, Y., Li, H.R., Yu, C.M., Li, P., Deng, X.M., Bian, J.J., Wang, J.F., 2023. PD-L1 promotes GSDMD-mediated NET release by maintaining the transcriptional activity of Stat3 in sepsis-associated encephalopathy. *Int. J. Biol. Sci.* 19, 1413–1429.